CHEMISTRY OF MATERIALS

pubs.acs.org/cm

Article

Synthesizing Mono- and Bimetallic 2D Selenophosphates Using a P_2Se_5 Reactive Flux

Eric K. Qian, Abishek K. Iyer, Matthew Cheng, Kevin M. Ryan, Lillian Jirousek, Daniel G. Chica, Patrick Krantz, Yea-Shine Lee, Venkat Chandrasekhar, Vinayak P. Dravid, and Mercouri G. Kanatzidis*

Cite This: *Chem. Mater.* 2023, 35, 3671−3685

Read Online

ACCESS | Metrics & More | Article Recommendations | Supporting Information

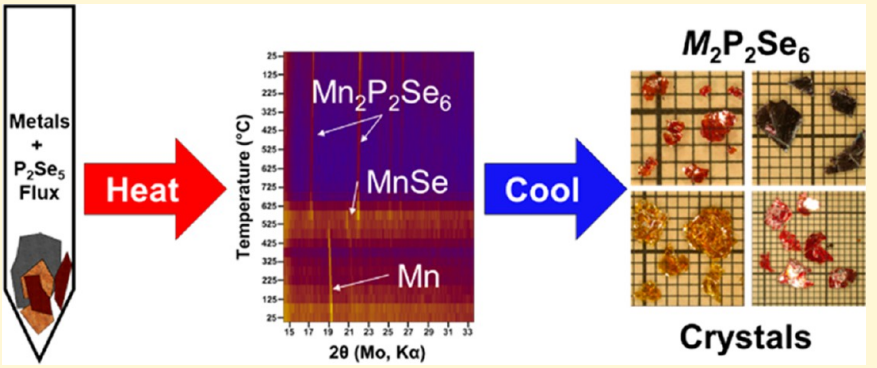

ABSTRACT: We have developed a new method for synthesizing mono- and bimetallic two-dimensional selenophosphates by using a reactive flux technique with powder precursors dissolved in a P_2Se_5 melt. This method allows us to bypass the difficulties commonly encountered in synthesizing these materials. $M_2P_2Se_6$ (M = Mn, Fe, Cr, Cd, Mg, and Zn) and bimetallic $MM'P_2Se_6$ (M = Cu, Ag; M′ = Cr, In) powders were synthesized over 60 h using a P_2Se_5 reactive flux. As a further demonstration of potential optimization, $Mn_2P_2Se_6$ powder with minor MnSe impurity was synthesized in 30 min. Reactions of Mn and Cr in P_2Se_5 flux were analyzed in situ using variable-temperature powder X-ray diffraction to investigate the formation reaction pathways, suggesting single-step formation of $Cr_2P_2Se_6$ at 775 °C and formation of $Mn_2P_2Se_6$ at 575 °C through an intermediate MnSe phase. Follow-up experimental syntheses generated crystals of the monometallic family $M_2P_2Se_6$ (M = Mn, Fe, and Cd) and bimetallic family $MM'P_2Se_6$ (M = Li, Cu, Ag; M′ = Cr, In) with area dimensions of several square millimeters using heating profiles of just over 60 h. The homogeneity of bimetallic selenophosphates $MM'P_2Se_6$ was confirmed using scanning electron microscopy, energy-dispersive X-ray spectroscopy, and Rietveld refinement. The crystallinity of the selected materials was characterized by transmission electron microscopy and atomic force microscopy measurements. The work functions of flakes were determined and ranged from 5.25 to 5.72 eV.

INTRODUCTION

Layered metal chalcophosphates $M_2P_2Q_6/MM'P_2Q_6$ (M = metal; Q = S, Se) are a family of two-dimensional (2D) materials initially discovered by Friedel in 1894[1]—recently, the family has attracted attention for use in 2D electronics. The magnetic and optical properties of these materials can be tuned through deliberate selection of the metals, garnering interest related to mapping and manipulation of magnetic and ferrielectric/ferroelectric ordering,[2−8] optoelectronics,[9] 2D stacked heterostructure devices,[10] hydrogen/oxygen evolution nanosheet electrocatalysts,[11−17] NO_x sensors,[18] and memristors.[19] $CuInP_2S_6$ has drawn special attention for its room-temperature ferrielectricity and bulk photovoltaic behavior at 315 K;[20] $Co_2P_2S_6$ has matched the overpotentials of IrO_2 and RuO_2 electrocatalysts for the oxygen evolution reaction;[15] and memristors with $Ag/M_2P_2S_6/Au$ architectures have been demonstrated with $Fe_2P_2S_6$, $Mn_2P_2S_6$, $Co_2P_2S_6$, and $Ni_2P_2S_6$.[21]

The layered $M_2P_2Q_6/MM'P_2Q_6$ family is suitable for such a wide array of applications due to the range of metals that can be accommodated in the octahedral sites of their structures.[22,23] Members of the layered metal chalcophosphate family primarily consist of 2D semiconductor slabs held together by weak van der Waals (vdW) forces. These slabs are composed of ethane-like $[P_2Q_6]^{4-}$ bipyramids, counter-

Received: February 14, 2023
Revised: April 9, 2023
Published: April 25, 2023

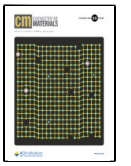

balanced by honeycomb arrangements of octahedrally coordinated cations (Figure 1)—the flexibility of the $[P_2Q_6]^{4-}$ polyanions allows the octahedral pocket to accommodate metals ranging from Li^+ to Bi^{3+}, so long as the average oxidation state is +2.

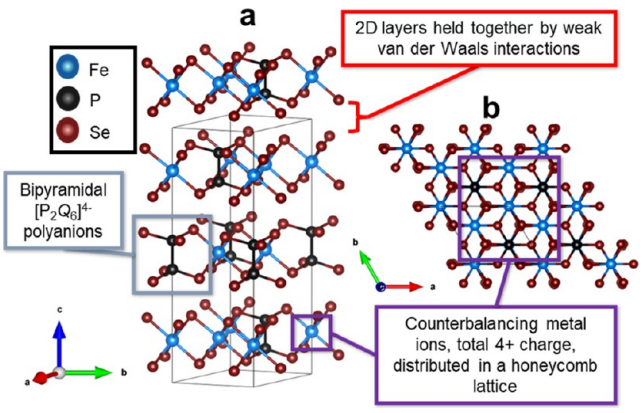

Figure 1. Crystal structure of $Fe_2P_2Se_6$, viewed (a) offset perpendicular to the *c* axis and (b) down the *c* axis. Crystal structures were generated using VESTA 3, using Crystallographic Information File provided by Klingen et al.[31,32]

The layered metal selenophosphates share the notable properties of the analogous thiophosphates: thus far, $CuInP_2Se_6$ has been reported as a ferrielectric[24] and $CuBiP_2Se_6$ and $AgBiP_2Se_6$ as antiferrielectric;[2] as for magnetic properties, $Fe_2P_2Se_6$, $Mn_2P_2Se_6$, $Ni_2P_2Se_6$, $CuCrP_2Se_6$, and $AgCrP_2Se_6$ have been observed to demonstrate antiferromagnetism, although the specific alignments do not appear to be reported.[25,26] However, the selenophosphates suffer from a lack of single-crystal studies. This void can likely be ascribed to unoptimized synthesis procedures for the selenophosphates. Published synthetic methods for monometallic $M_2P_2Se_6$ materials traditionally involve self-transport through direct stoichiometric combination in sealed ampoules, with reaction times ranging from a few days to a few months.[27−33] Modern studies favor iodine-assisted chemical vapor transport of elements, which may require 4−7 days of controlled transport in a multi-zone furnace—the technique is remarkable for crystal growth quality but is disadvantaged when trying to synthesize elementally complex multinary phases or scaling up to larger reaction amounts.[21,22,34] Some bimetallic $MM'P_2Se_6$ materials have been synthesized using traditional solid-state ceramic methods but still require 2 or 3 week reactions.[30] A summary of current layered metal selenophosphate syntheses is tabulated in Table 1. Finding a rapid synthesis of these materials would relieve a synthetic bottleneck and unlock a complementary branch of 2D selenophosphate properties and device research.

Chica et al. reported rapid crystal growth of $M_2P_2S_6$ materials using a reactive P_2S_5 flux.[35] In contrast to the standard solid-state ceramic method, molten flux reactions increase diffusion by establishing an oxidizing liquid reaction medium, which solvates metal reactants at lower temperatures. Reactive fluxes provide the additional benefit of incorporating themselves into the final product, further improving reagent incorporation. Some fluxes can also react with unwanted competing products, enhancing the yield and purity of the final product.[36] The use of a reactive P_2S_5 flux has been

Table 1. Published Literature Synthesis Profiles for Layered Metal Selenophosphates[a]

compound	temperature/duration	reactants	references
$Mn_2P_2Se_6$	DC: 650 °C, 10 days	Mn, P, Se	15
	DC: 650 °C, 7 days	Mn, P, Se	17
	CVT: 700−650 °C, 7 days, I_2 transport	Mn, P, Se	18
	CVT: 650−610 °C, 7 days, I_2 transport	Mn, P, Se	21
	CVT: 600−650 °C, 10 days, I_2 transport	Mn, P, Se	24
	DC: 650 °C, 10 days	Mn, P, Se	25
	DC: 600−720 °C, 2 months	Mn, P, Se	28
$Fe_2P_2Se_6$	DC: 650 °C, 10 days	Fe, P, Se	15
	DC: 650 °C, 7 days	Fe, P, Se	17
	CVT: 650−610 °C, 7 days, I_2 transport	Fe, P, Se	21
	DC: 550−700 °C, 2 months	Fe/FeSe, P, Se	28
	CVT: 650−610 °C, unreported, Cl_2 transport	Fe, P, Se	29
$Cr_2P_2Se_6$	DC: 650 °C, 10 days	Cr, P, Se	24
$Zn_2P_2Se_6$	CVT: 370 °C, 10 days, I_2 transport	Zn, P, Se	15
	CVT: 370 °C, 10 days, I_2 transport	Zn, P, Se	25
	CVT: 300 °C, 4 days, I_2 transport	Zn, P, Se	39
$Ni_2P_2Se_6$	DC: 500−560 °C,3 months	Ni, P, Se	26
$Cd_2P_2Se_6$	DC: 650 °C, 10 days	Cd, P, Se	15
	DC: 650 °C, 7 days	Cd, P, Se	17
	DC: 650 °C, 10 days	Cd, P, Se	25
	DC: 550−650 °C, 1 month	Cd, P, Se	28
$AgInP_2Se_6$	DC: 750 °C, 10 h; then annealed at 500 °C, 14 days	Ag, In, P, Se	27
	CVT: 600−775 °C (50 °C gradient), 4 days	Ag, In, P, Se	22
$CuInP_2Se_6$	DC: 750 °C,10 h; then annealed at 500 °C, 14 days	Cu, In, P, Se	27
	CVT: 600−775 °C (50 °C gradient), 4 days	Cu, In, P, Se	22
$AgCrP_2Se_6$	DC: 750 °C, 10 h; then annealed at 600 °C, 21 days	Ag, Cr, P, Se	27
$CuCrP_2Se_6$	DC: 750 °C, 10 h; then annealed at 550 °C, 21 days	Cu, Cr, P, Se	27

[a]Reactions are labeled as direct combination/self-transport (DC) or chemical vapor transport (CVT).

demonstrated to reduce synthesis time for $Ni_2P_2S_6$ to 1 h for powder or up to 3 days for crystals 1−7 mm^2 in size.[35]

An extensive investigation of the analogous $M_2P_2Se_6$ or $MM'P_2Se_6$ synthesis using a P_2Se_5 flux has not yet been published. In 2003, Galdámez et al. synthesized $MM'P_2Se_6$ (M = Cu, Ag; M′ = Sb, Bi) compounds using a 1:1:1.5:2.0 ratio of M, M′, P_2Se_5, and Se but had not expanded use of the P_2Se_5 flux to other metal selenophosphates.[37] Other reports of flux syntheses of related materials are primarily the synthesis of alkali metal chalcophosphates in alkali metal salt fluxes.[29,38]

Herein, we report the analogous P_2Se_5 flux-mediated method for rapid synthesis and crystal growth of layered mono- and bimetallic selenophosphates. We devised various synthesis procedures for synthesizing $M_2P_2Se_6$ (M = Mn, Fe, Cr, Cd, Mg, and Zn) and bimetallic $MM'P_2Se_6$ (M = Cu, Ag; M′ = Cr, In) powders in 60 h or less. We explored various methods of P_2Se_5 flux removal, ultimately relying on a distillation setup using a temperature gradient between 400 °C and room temperature. Variable-temperature (VT)-powder X-ray diffraction (PXRD) in situ measurements on mono-

https://doi.org/10.1021/acs.chemmater.3c00342
Chem. Mater. 2023, 35, 3671−3685

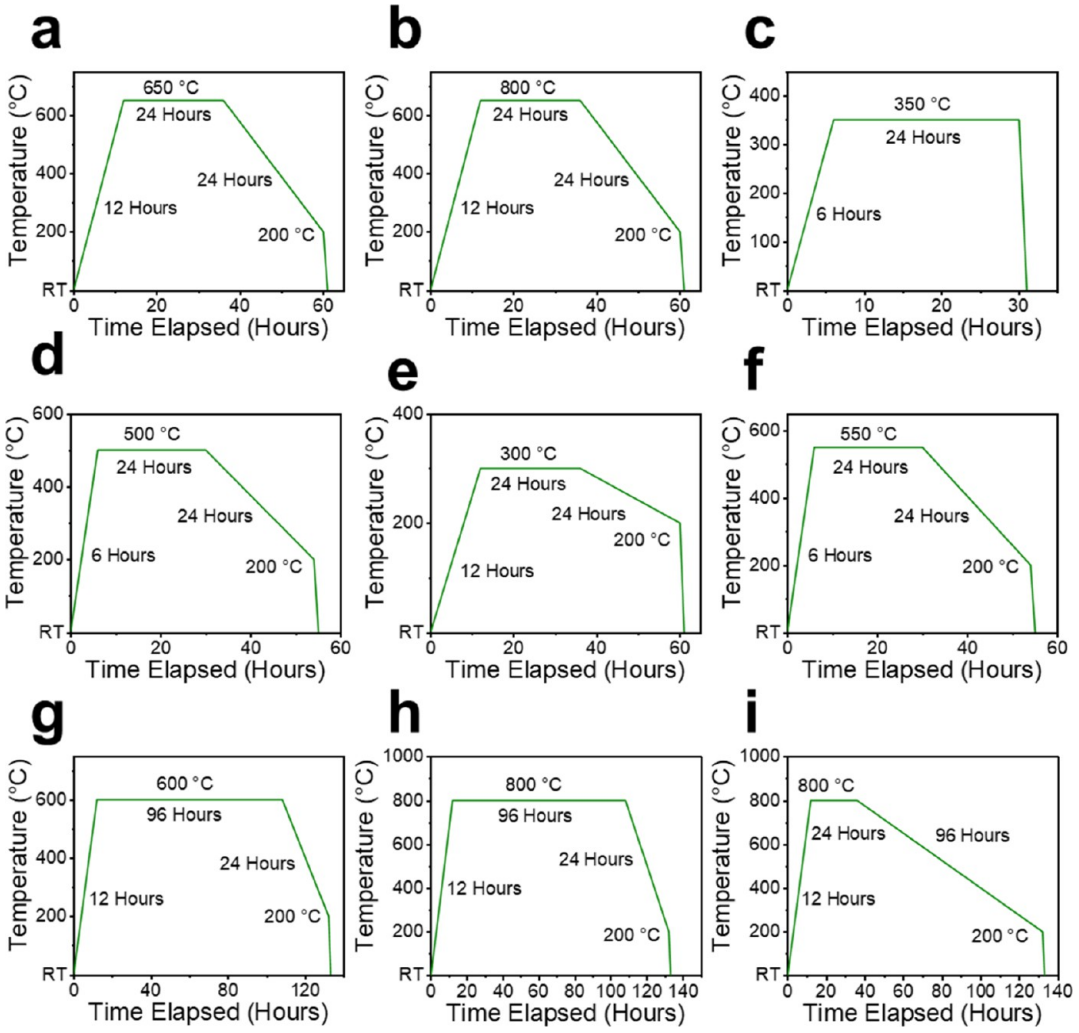

Figure 2. Heating profiles used for (a) general synthesis of layered metal selenophosphate powders, (b) general synthesis of layered metal selenophosphate crystal flakes, (c) P_2Se_5 flux removal by distillation, (d) adjusted synthesis for $Ni_2P_2Se_6$ powder, (e) adjusted synthesis for $Zn_2P_2Se_6$, (f) adjusted synthesis for $Mg_2P_2Se_6$ and $Ni_2P_2Se_6$, (g) polycrystalline synthesis of bimetallic $MM'P_2Se_6$ compounds, (h) experimentally extended dwell duration for crystal growth optimization, and (i) experimentally extended cooling duration for crystal growth optimization.

metallic selenophosphates suggest one-step formation of $Cr_2P_2Se_6$ from the Cr/P_2Se_5 reaction and formation of $Mn_2P_2Se_6$ from Mn/P_2Se_5 via two pathways: (1) one-step formation from Mn to $Mn_2P_2Se_6$ or (2) by the MnSe intermediate phase. Follow-up experiments with a pre-heated furnace revealed that powder $Mn_2P_2Se_6$ could be synthesized as quickly as 30 min in a molten P_2Se_5 flux. Experimental syntheses of $M_2P_2Se_6/MM'P_2Se_6$ materials at 800 °C for 24 h with additional excess P_2Se_5 flux using a 60 h heating profile produced large (>1 mm^2) crystalline flakes, larger than crystals grown in 4−7 days of chemical vapor transport.[21,22]

EXPERIMENTAL SECTION

Reagents. Manganese powder (Mn, 99.5%, Alfa Aesar), iron powder (Fe, 99.9%, Cerac), cobalt powder (Co, 99.8%, Cerac), nickel powder (Ni, 99.9%, Johnson Matthey), copper powder (Cu, 99.999%, Sigma-Aldrich), zinc powder (Zn, 99.9%, Sigma-Aldrich), cadmium powder (Cd, 99.9999%, Cerac), indium droplets (In, 99.9%, Aldrich), phosphorous pieces (P, 99.999%, Puratronic Alfa Aesar), and selenium shot (Se, 99.999%, Puratronic Alfa Aesar) were used as purchased without additional purification.

Synthesis of the P_2Se_5 Precursor. Red phosphorous pieces (0.6781 g, 21.89 mmol) and selenium shot (4.3219 g, 54.74 mmol) were layered into 8 in.-long fused silica tubes (outer diameter of 12.7 mm and inner diameter of 10.5 mm), with the selenium on the bottom. The tube was then evacuated to a pressure of 3.2×10^{-3} mbar and flame-sealed with an oxygen/natural gas torch to a length of ∼6 in. After the tube had cooled, the reagents were physically mixed by shaking the tube for 1 min. The tube was then loaded into a tube furnace and heated using the following temperature profile: a 12 h ramp from room temperature to 500 °C, a 72 h dwell at 500 °C, and then the furnace cooling to room temperature. The tubes were opened in an ambient atmosphere, but P_2Se_5 was stored in a nitrogen-filled glovebox.

Synthesis of $Mn_2P_2Se_6$ Powder. Powdered $Mn_2P_2Se_6$ was synthesized in a 2 Mn: 3 P_2Se_5 flux ratio. 0.0742 g (1.351 mmol) of Mn powder and 0.9258 g (2.027 mmol) of P_2Se_5 pieces were charged into 8 in.-long fused silica tubes (outer diameter of 12.7 mm and inner diameter of 10.5 mm) lined with Al foil to minimize powder coating on the inside walls of the tube. The reagents were mixed by lightly shaking and tapping the walls of the tube for 10 s; after sufficient mixing, the Al foil liner was removed. The tube was evacuated to a pressure of 4.0×10^{-3} mbar and flame-sealed with an oxygen/natural gas torch to a length of ∼6 in. The tube was then loaded into a computer-controlled tube furnace using the heating profile shown in Figure 2a. Detailed synthesis procedures for other powdered $M_2P_2Se_6/MM'P_2Se_6$ materials are provided in the Supporting Information.

https://doi.org/10.1021/acs.chemmater.3c00342
Chem. Mater. 2023, 35, 3671−3685

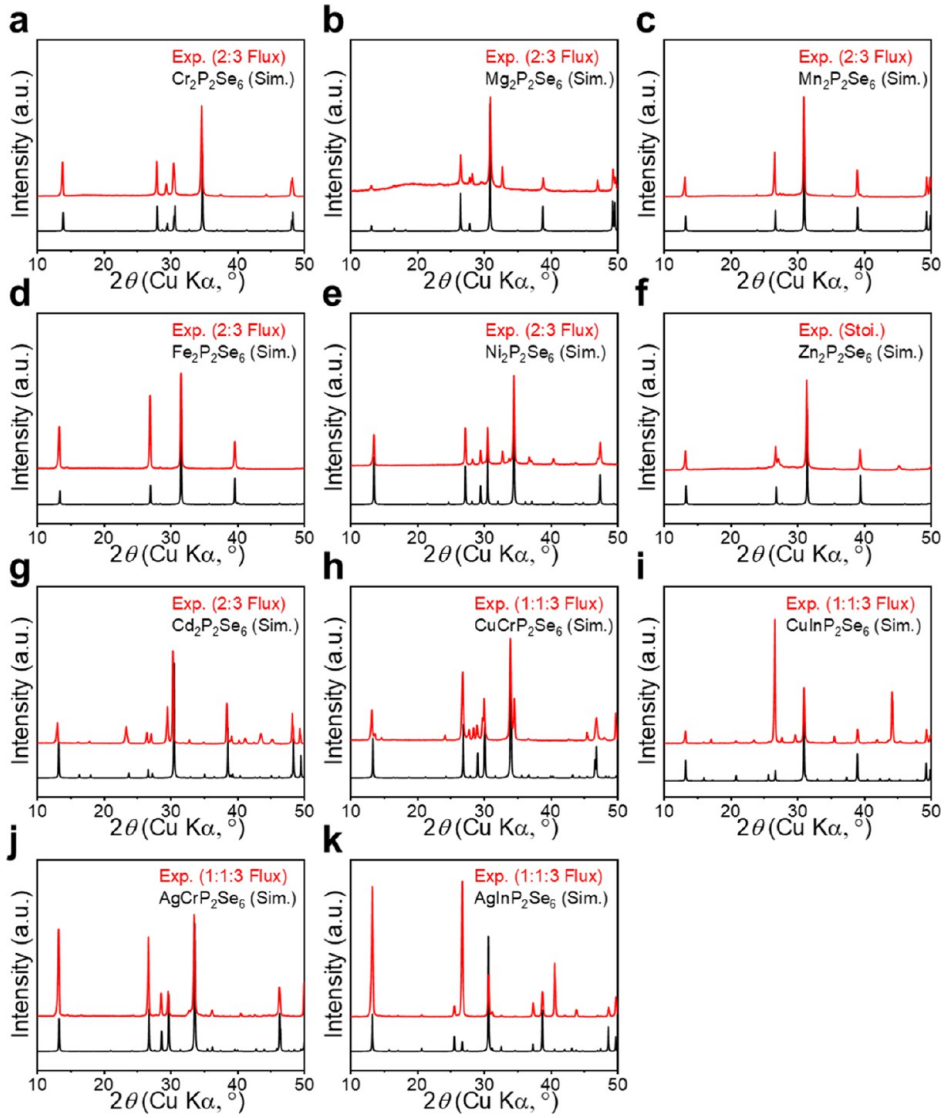

Figure 3. Monometallic and bimetallic selenophosphate PXRD comparisons between simulated patterns (in black) and observed patterns obtained from (a) $Cr_2P_2Se_6$ powder, (b) $Mg_2P_2Se_6$ powder (MgSe impurity), (c) $Mn_2P_2Se_6$ powder, (d) $Fe_2P_2Se_6$ powder, (e) $Ni_2P_2Se_6$ powder (NiP_2 impurity), (f) $Zn_2P_2Se_6$ powder, (g) $Cd_2P_2Se_6$ powder (Se impurity), (h) polycrystalline $CuCrP_2Se_6$ (Cu_3PSe_4 and Cr_2Se_3 impurities), (i) polycrystalline $CuInP_2Se_6$ ($CuInSe_2$ impurity), (j) polycrystalline $AgCrP_2Se_6$, and (k) polycrystalline $AgInP_2Se_6$ synthesized using 2 M: 3 P_2Se_5 or 1 M: 1 M′: 3 P_2Se_5 flux ratios.

Synthesis of $Mn_2P_2Se_6$ Crystalline Flakes. Crystalline flakes of $Mn_2P_2Se_6$ were synthesized in a 2 Mn: 15 P_2Se_5 flux ratio. 0.0314 g (0.572 mmol) of Mn powder and 2.0226 g (4.4283 mmol) of P_2Se_5 pieces were ground together for about 1 min with a mortar and pestle in air until visually fine and homogenized and then charged into 8 in.-long fused silica tubes (outer diameter of 12.7 mm and inner diameter of 10.5 mm) lined with Al foil to minimize powder coating on the inside walls of the tube. The Al foil liner was removed after charging. The tube was evacuated to a pressure of 3.2×10^{-3} mbar and flame-sealed with an oxygen/natural gas torch to a length of ∼6 in. The tube was then loaded into a computer-controlled tube furnace using the heating profile shown in Figure 2b. Detailed synthesis procedures for other crystalline $M_2P_2Se_6$/$MM'P_2Se_6$ materials are provided in the Supporting Information.

Removal of Excess P_2Se_5 Flux from Reaction Products. For both powder and crystalline syntheses, after the initial heating, the ampoules were opened, and the ingots were loaded into new 12 in.-long fused silica tubes with outer diameters of 15 mm and inner diameters of 13 mm. No Al foil liners were used for this step. The tubes were then evacuated again to a pressure of 3.2×10^{-3} mbar and flame-sealed to a length of ∼10 in. For the second heating step, the tubes were placed in a tube furnace with the ingot-containing end adjacent to the thermocouple in the center of the tube furnace and the other end sticking out of the furnace, air-cooled to room temperature. Insulation was placed only to the edge of the tube furnace. A picture of the setup is available in Figure S1. The tubes were then heated under the P_2Se_5 removal conditions shown in Figure 2c. This setup generated a temperature gradient between 350 °C and room temperature, causing volatilization of excess P_2Se_5 to condense on the colder end of the tube sticking out of the furnace. This distillation of P_2Se_5 was repeated 1−3 times until all the P_2Se_5 red−black glass was visibly removed. Occasionally, excess P_2Se_5 in powdered $M_2P_2Se_6$/$MM'P_2Se_6$ would condense on the top end of the reaction tube during the cooling step of the initial synthesis, eliminating the need for removal.

Variable-Temperature Powder X-ray Diffraction. A STOE STADI MP high-resolution diffractometer was used to study Mn/P_2Se_5 and Cr/P_2Se_5 reactions. For the Mn/P_2Se_5 reaction, pure-Mo Kα1 radiation (0.70930 Å) operated at 50 kV and 40 mA was used; for the Cr/P_2Se_5 reaction, pure-Ag Kα1 radiation (0.55941 Å) operated at 40 kV and 40 mA was used. The diffractometer uses an asymmetrically curved germanium monochromator to select the

https://doi.org/10.1021/acs.chemmater.3c00342
Chem. Mater. 2023, 35, 3671−3685

appropriate Kα1 line and has a one-dimensional silicon strip detector (MYTHEN 2 1K, DECTRIS). Prior to measurement, calibration was performed using a NIST silicon standard (640 d).

In the ambient atmosphere, P_2Se_5 chunks were ground and sieved to a particle size of <53 μm, added to −325 mesh metal powders in a 2 M: 3 P_2Se_5 ratio to a total mass of 0.500 g, and then ground in an agate mortar and pestle for 2 min. Mixed M/P_2Se_5 powders were packed into a fused quartz capillary (0.7 mm capillary for Mn/P_2Se_5, 0.5 mm capillary for Cr/P_2Se_5) and then evacuated to $\sim 3 \times 10^{-3}$ mbar and flame-sealed. The capillary was then placed in the furnace attachment (0.1 °C temperature stability) of the STOE STADI MP diffractometer. The samples were spun during the collection. In each experiment, the furnace was ramped at 200 °C/h, with a stationary detector collecting PXRD patterns every 50 °C, with a 2θ (Mo/Ag, Kα1) angle range of approximately 17°. The complete heating profiles used during collection are shown in Figure S2.

Powder X-ray Diffraction. PXRD patterns were taken using reflection geometry with a Rigaku Miniflex 5600 powder X-ray diffractometer with Ni-filtered Cu Kα radiation (λ = 1.5406 Å) with a 40 kV voltage and 15 mA current. The diffraction pattern scan width was 0.02° with a 2θ range between 5 and 90°, scanned at 15°/min. Preferred orientation was reduced by using a welled, zero background sample holder and spinning the sample during data collection. Simulated PXRD patterns were generated using Mercury software.[39] The lattice parameters were determined using Rietveld refinement through GSAS II.[40]

SEM−EDS Analysis of Bimetallic $MM'P_2Se_6$ Flakes. Scanning electron microscopy (SEM)−energy-dispersive X-ray spectroscopy (EDS) was used to confirm the elemental composition of the bimetallic layered metal selenophosphate $MM'P_2Se_6$ samples. Data were obtained with a Hitachi S-3400 VP-SEM with an accelerating voltage of 40 kV and a probe current of 50 μA on flakes affixed onto a SEM stub with carbon tape. Spectra were taken from multiple areas on each flake, with output count rates around 2000 cps, for 10 s each. The EDS spectra were collected using an Oxford INCAx-act EDS system. The spectra were analyzed using Oxford Instruments AZtec software. The signal from carbon was excluded. The atomic percentage of Li in $LiInP_2Se_6$ was unable to be confirmed, as the characteristic Li K X-ray emissions are weak and easily absorbed before detection, resulting in an insufficient signal.

Transmission Electron Microscopy (TEM) Imaging, Selected-Area Electron Diffraction (SAED), and Scanning Transmission Electron Microscopy−Energy-Dispersive X-ray Spectroscopy (STEM−EDS). High-resolution transmission electron microscopy (HRTEM) and selected-area electron diffraction (SAED) were obtained with a JEOL ARM300 microscope at 300 kV along the [0001]-zone axis to ascertain the crystalline nature of $Mn_2P_2Se_6$, $Fe_2P_2Se_6$, and $AgInP_2Se_6$. Scanning TEM (STEM) X-ray energy-dispersive spectroscopy (XEDS) was conducted with an Oxford silicon drift detector to determine stoichiometry and chemical distribution of $Mn_2P_2Se_6$, $Fe_2P_2Se_6$, and $AgInP_2Se_6$. The convergence angle of the STEM probe is 24 mrad which at 300 keV corresponds to a probe size of 0.57 Å. Full width at half-maximum (fwhm) and the solid angle of the Oxford detector are 0.98 sr. TEM samples were prepared using liquid exfoliation in ethanol. SAED patterns were simulated with SingleCrystal.[41]

Photoemission Yield Spectroscopy in Air (PYSA). Photoemission yield spectroscopy in air (PYSA) (AC-2, Riken-Keika) was used to measure the work function of powdered samples. For semiconductors, the work function is equal to the valence band maximum with respect to the vacuum energy. The sample was illuminated by a tunable monochromatic ultraviolet light source (UV, 4.50−6.20, 0.10 eV step increments) under dry air. At each excitation energy step, if the incident photon energy was higher than the work function, photoelectrons were measured. The work function values were determined as the linear onset of the PYSA spectra for each material.

RESULTS AND DISCUSSION

Synthesis of Layered Metal Selenophosphate Powders. Experimental synthesis was initially conducted to synthesize $Cr_2P_2Se_6$, $Mn_2P_2Se_6$, and $Fe_2P_2Se_6$. Chica et al. reported using the following temperature profile to synthesize 14 members of the metal thiophosphate family: a 10 h ramp from room temperature to 650 °C, a 36 h dwell at 650 °C, a 12 h cool to 250 °C, and then the furnace was allowed to cool to room temperature.[35] Theorizing that the dwell duration could be shortened and that increasing cooling duration could improve crystal formation, the following furnace profile was devised: a 12 h ramp from room temperature to 650 °C, a shortened 24 h dwell at 650 °C, an extended 24 h cool to 200 °C, and then allowing the furnace to cool to room temperature (Figure 2a). This profile immediately proved successful in synthesizing pure powders of $Cr_2P_2Se_6$, $Mn_2P_2Se_6$, and $Fe_2P_2Se_6$ (Figure 3a,c,d, respectively).

Follow-up attempts to synthesize $Ni_2P_2Se_6$ and $Zn_2P_2Se_6$ under the same conditions failed, resulting in the complete formation of $NiSe_2$ and ZnSe (Figure S3a,b). In their initial report of these compounds, Klingen et al. and Hahn reported growing $Mn_2P_2Se_6$ and $Fe_2P_2Se_6$ within the following temperature gradients: $Mn_2P_2Se_6$ at 600−720 °C and $Fe_2P_2Se_6$ at 550−700 °C, with both ranges falling within our dwell temperature of 650 °C.[31] Their synthesis of $Ni_2P_2Se_6$ was conducted at 500−560 °C; thus, our reaction likely overheated and degraded into $NiSe_2$. Attempting another synthesis of $Ni_2P_2Se_6$ with a dwell temperature of 500 °C (Figure 2d) resulted in pure formation of $Ni_2P_2Se_6$ powder. For $Zn_2P_2Se_6$, Jörgens and Mewis reported a synthesis of $Zn_2P_2Se_6$ at 300 °C using an I_2 mineralizer, with ZnSe and P_4Se_4 impurities, noting higher impurity concentrations from syntheses at higher temperatures.[29] Although P_2Se_5 successfully formed a reactive molten flux at 300 °C, our flux removal method required heating at 350 °C or above. A 300 °C $Zn_2P_2Se_6$ flux-based synthesis followed by a 350 °C excess P_2Se_5 distillation was attempted, but the reaction produced $Zn_2P_2Se_6$ with significant ZnSe impurities (Figure S3c). Bypassing the need for P_2Se_5 flux removal, a 300 °C stoichiometric synthesis under the conditions listed in Figure 2e was attempted, producing gray, red, and orange pieces of $Zn_2P_2Se_6$. The color gradient depended on the amount of ZnSe impurity present (Figure S4). Rietveld refinement (Figure S14) on the PXRD pattern (Figure 3f) taken from one of the gray pieces calculated a 97.1% $Zn_2P_2Se_6$/2.9% ZnSe split, by the weight percentage.

P_2Se_5 flux-based investigations were resumed for the synthesis of $Mg_2P_2Se_6$ (reported synthesis at 700 °C)[42] and $Cd_2P_2Se_6$ (reported synthesis at 550−650 °C).[31] Once again, targeting the lower temperatures within these ranges proved successful; powders of both compounds could be synthesized in the P_2Se_5 flux at 550 °C (Figure 2f), with impurities. Rietveld refinement (Figures S15 and S16) of the PXRD patterns (Figure 3b,g) showed 38.2 wt % Se and 15.1 wt % MgSe impurities. Normally, a 38.2 wt % of Se contamination would be particularly alarming. However, the P_2Se_5 flux removal process freezes droplets of Se to the walls of the tube during distillation; it is suspected that some of these droplets were ground together with $Cd_2P_2Se_6$ while preparing the PXRD samples.

In addition to the known monometallic compositions, some known bimetallic compounds were explored as well, using the same profile that was used to synthesize $Mn_2P_2Se_6$ (Figure 2a).

https://doi.org/10.1021/acs.chemmater.3c00342
Chem. Mater. 2023, 35, 3671−3685

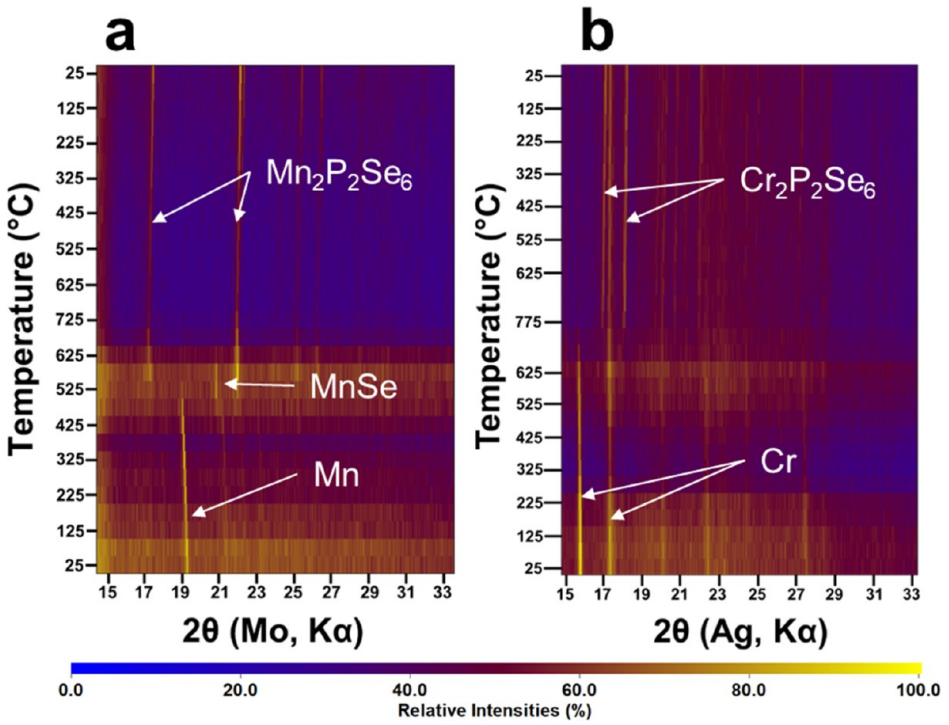

Figure 4. VT-PXRD patterns for (a) Mn/P_2Se_5 and (b) Cr/P_2Se_5 reactions. PXRD patterns were collected every 50 °C, from 25 to 725 °C for the Mn/P_2Se_5 system and 25−775 °C for the Cr/P_2Se_5 system. Consumption of reactants to form products causes certain peaks to lose intensity as others gain intensity, providing insights into the mechanisms at play.

The $Cu/Cr/P_2Se_5$ system formed some polycrystalline $CuCrP_2Se_6$ but was primarily dominated by Cu_3PSe_4 and Cr_2Se_3 impurities (Figure S5a). Similarly, the $Ag/Cr/P_2Se_5$ system formed some polycrystalline $AgCrP_2Se_6$ but was heavily contaminated with $Ag_4P_2Se_6$ and Cr_2Se_3 (Figure S5c). In contrast, the $Cu/In/P_2Se_5$ system formed polycrystalline $CuInP_2Se_6$ as the major product, with minor $CuInSe_2$ contamination (Figure S5b), and the $Ag/In/P_2Se_5$ system successfully formed pure-phase polycrystalline $AgInP_2Se_6$ (Figure S5d) on first attempt. It was determined that the undesired binary and ternary contaminants could be a result of inadequate time during the dwell period to fully react or degradation due to excessively high reaction temperatures. To potentially bypass both problems, a reaction profile with a 4 day dwell at 600 °C (Figure 2g) was used to explore all four of these systems further. The $Cu/Cr/P_2Se_5$ system showed the improved formation of $CuCrP_2Se_6$, but was still heavily contaminated with impurities, this time from $Cr_2P_2Se_6$ and $CuCr_2Se_4$. The PXRD pattern compared to the simulated $CuCrP_2Se_6$ pattern is shown in Figure 3h, whereas a breakdown of the contaminants is available in Figure S6a. Neither the $Cu/In/P_2Se_5$ system nor the $Ag/In/P_2Se_5$ system showed any improvements from the extended dwell period; however, $Ag/Cr/P_2Se_5$ completely formed pure $AgCrP_2Se_6$ (Figure 3k). Overall, it was demonstrated that by using a P_2Se_5 reactive flux, many $M_2P_2Se_6/MM'P_2Se_6$ materials could be synthesized in the powder or polycrystalline form in 60 h or less.

Removal of Excess P_2Se_5 Flux from Reaction Products. All flux-mediated reactions introduced an additional challenge in the form of excess P_2Se_5 flux removal after reaction completion. Excess P_2S_5 flux in the synthesis of metal thiophosphates can be washed away with a heated mixture of 50:50 (v/v) deionized water and ethanol. However, similar attempts with P_2Se_5 showed no degradation in the mixture. A P_2Se_5 flux-based synthesis of β-$Bi_4(P_2Se_6)_3$ by Aitken et al. reported using a combination of *N*,*N*-dimethylformamide (DMF) and ethylenediamine to wash away excess P_2Se_5.[43] To check metal selenophosphate stability in these solvents, $Mn_2P_2Se_6$ samples were rinsed with DMF, ethylenediamine, and a combination of the two. PXRD analysis showed that washes with ethylenediamine resulted in the addition of low-angle peaks around $2\theta = 7°$, suggesting a superlattice due to ethylenediamine intercalating between the $Mn_2P_2Se_6$ layers (Figure S7a). A look at Clément publications in the 1990s reveals significant research into the organic intercalation of layered metal chalcophosphates, including an example of tetramethylammonium intercalation into $M_2P_2S_6$.[44,45] Regardless, the washing capabilities of the 3 DMF: 1 ethylenediamine mixture was also tested on an ingot of Zn/P_2Se_5 that had been reacted at 300 °C. The P_2Se_5 content, which is manifested in the PXRD pattern as broad-peaked intensity around $2\theta = 20$, 30°, showed no changes, suggesting that the DMF/ethylenediamine mixture was ineffective at dissolving the excess P_2Se_5 flux (Figure S7b).

As an alternative, due to the low melting point of P_2Se_5 (214 °C),[46] the excess P_2Se_5 flux could also be boiled off. By sealing a P_2Se_5-rich ingot in a long sealed ampoule, the ingot could be held at 350 or 400 °C inside of a furnace while exposing the other side of the ampoule to room temperature. This establishes a temperature gradient that continually volatilizes excess P_2Se_5 and condenses it on the other end of the ampoule. Most $M_2P_2Se_6/MM'P_2Se_6$ materials are stable at these lower temperatures, resulting in a flux removal process that does not risk degradation or alteration of the desired product.

In Situ PXRD Measurements. The reaction pathways for the formation of $Mn_2P_2Se_6$ and $Cr_2P_2Se_6$ were further investigated using VT in situ PXRD between 25 and 775 °C.

https://doi.org/10.1021/acs.chemmater.3c00342
Chem. Mater. 2023, 35, 3671−3685

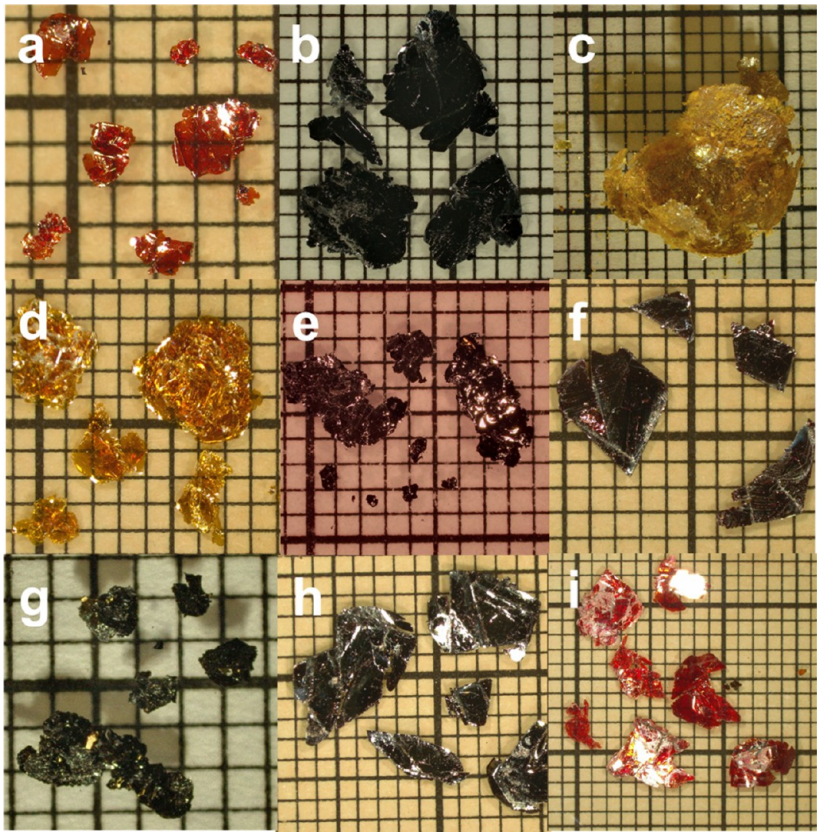

Figure 5. Optical images of (a) $Mn_2P_2Se_6$, (b) $Fe_2P_2Se_6$, (c) $Zn_2P_2Se_6$, (d) $Cd_2P_2Se_6$, (e) $CuCrP_2Se_6$, (f) $CuInP_2Se_6$, (g) $AgCrP_2Se_6$, (h) $AgInP_2Se_6$, and (i) $LiInP_2Se_6$ flakes on square mm grid paper. Samples are slightly elevated on 1 mm thick glass microscope slides. Crystals were grown over 60 h, using the heating profile shown in Figure 2b.

The PXRD patterns collected during the Mn/P_2Se_5 reaction are compiled in Figure 4a, with a 2θ (Mo, Kα1) range of 14.7−33.18°. Between the patterns collected at 475 and 525 °C during the heating cycle, the characteristic Mn peak at 2θ = 19° loses intensity upon the growth of $Mn_2P_2Se_6$ peaks at 2θ = 17.5 and 22°, with minor MnSe impurities showing at 2θ = 21°. This suggests consumption of Mn metal to form $Mn_2P_2Se_6$, with MnSe competing as a formation product. The MnSe peak noticeably weakens by 625 °C, suggesting consumption of MnSe to also form $Mn_2P_2Se_6$; however, it is unclear if this resulted from additional reaction time or increased temperature. $Mn_2P_2Se_6$ then remained stable in the flux as the reaction cooled back to room temperature.

The PXRD patterns collected during the Cr/P_2Se_5 reaction are compiled in Figure 4b, with a 2θ range of 14.7 and 33.18°. Between the patterns collected at 675 and 775 °C during the heating cycle, the Cr peaks at 2θ = 15.5 and 17° disappear concurrently with the growth of $Cr_2P_2Se_6$ peaks at 2θ = 16.5, 17, and 18°. This suggests the consumption of Cr metal to directly form $Cr_2P_2Se_6$, bypassing the formation of any parasitic or intermediary binary products. Together, both in situ PXRD experiments indicate that some metal powders in P_2Se_5 flux have the potential to form $M_2P_2Se_6$ phases without any intermediary phases, whereas others may competitively form metal selenides. It is speculated that this could be related to kinetic and/or thermal stabilities of certain binary M_xP_y and M_xSe_y products. For example, one possibility is that the formation of MnSe is kinetically equal or advantageous to the formation of $Mn_2P_2Se_6$ but that the formation of CrSe or Cr_2Se_3 may be kinetically disadvantageous compared to the formation of $Cr_2P_2Se_6$—thus, an indirect formation of $Mn_2P_2Se_6$ (or concurrent formation of MnSe and $Mn_2P_2Se_6$) would be observed, in contrast to a direct formation of $Cr_2P_2Se_6$.

However, those parasitic metal selenides may react further with the P_2Se_5 molten flux to form the target $M_2P_2Se_6$ phase, ultimately resulting in a phase-pure final product. Thus, a possible approach to eliminating binary or ternary impurities would be to increase reaction temperature—at the risk of product degradation—or to increase reaction time, as evidenced by the improvements in purity for the $Ag/Cr/P_2Se_5$ reactions.

A Co/P_2Se_5 reaction was similarly investigated to see if $Co_2P_2Se_6$ could be formed by a similar pathway, despite not being previously reported. However, no obvious formation of $Co_2P_2Se_6$ was observed (Figure S28). It is important to note that $Co_2P_2S_6$ can form but degrades into Co(PS) at higher temperatures.[35] It is possible that $Co_2P_2Se_6$ does form but also degrades into Co(PSe) or Co_xP_y/Co_xSe_y binaries at higher temperatures—this reveals one of the weaknesses in comparing VT PXRD to furnace reactions since the two experiments do not really possess exactly the same conditions, in that VT PXRD occurs at much faster rates. This investigation could be further supported by a combination of energy calculations for the formation of $Co_2P_2Se_6$ vs Co_xP_y/Co_xSe_y, slower VT PXRD measurements, and variation in dwell temperatures.

Discussion on the Mechanism of the P_2Se_5 Reactive Flux. As shown in Figure 1, the layered metal selenophosphates consist of octahedrally coordinated 2+ cations sandwiched between polyanionic $[P_2Se_6]^{4-}$ units. The

https://doi.org/10.1021/acs.chemmater.3c00342
Chem. Mater. 2023, 35, 3671−3685

conditions for forming these materials with elemental reactants are twofold: (1) the phosphorus and selenium should preferentially bond to each other over forming metal phosphides or metal selenides, and (2) the metals need to react in a sufficiently oxidizing environment. As with the use of P_2S_5 flux in the synthesis of layered metal thiophosphates, the excess P_2Se_5 reactive flux appears to address both problems by (1) providing a P−Se binary as a reactant, discouraging M_xP_y or M_xSe_y formation and (2) serving as strong Lewis acids that oxidize the metal(s) of interest and increase their solubility.

Based on the rapid formation of $Mn_2P_2Se_6$ shown in the in situ PXRD measurements, an experiment was set up to experimentally synthesize $Mn_2P_2Se_6$ on a larger scale within 30−60 min using a tube furnace pre-heated to 650 °C. Four 2 g Mn/P_2Se_5 reactions were loaded into 8 in. long fused silica tubes (12.5 mm outer diameter, 10.7 mm inner diameter) lined with Al foil and then flame-sealed with an oxygen/natural gas torch to a length of 6 in.: (1) 0.0739 g (0.135 mmol) of Mn powder finely ground together with 0.9501 g (0.2080 mmol) of P_2Se_5 pieces; (2) 0.0740 g (0.135 mmol) of Mn powder layered under 0.9565 g (0.2094 mmol) of P_2Se_5 pieces; (3) 0.0741 g (0.135 mmol) of Mn powder finely ground together with 1.0107 g (0.2213 mmol) of P_2Se_5 pieces; and (4) 0.0744 g (0.135 mmol) of Mn powder layered under 0.9736 g (0.2131 mmol) of P_2Se_5 pieces. All four ampoules were loaded into a pre-heated furnace. Then, one ampoule of each preparation method was removed and air-quenched at 30 min and at 1 h of heating. The products were then ground and analyzed using PXRD, as shown in Figure 6a−d.

Although the difference is minor, the 30 and 60 min ground samples had a lower MnSe content than their not-ground counterparts. Comparison between the not-ground 30 and 60 min sample PXRD patterns supports the hypothesis from the in situ PXRD measurements: the 30 min sample (Figure 6a) features both broad P_2Se_5 amorphous peaks and sharp MnSe peaks, whereas the 60 min sample (Figure 6b) has no P_2Se_5 peaks, less intense MnSe peaks, and more intense $Mn_2P_2Se_6$—within those additional 30 min of heating, P_2Se_5 and MnSe were consumed to form $Mn_2P_2Se_6$. Further comparison of these two patterns with the PXRD pattern of the ground 30 min sample (Figure 6c) also reveals two more important details: (1) at 650 °C, P_2Se_5 is not sufficiently fluid enough to solvate and mix all of the reactants in 30 min but can do so within 60 min, and (2) grinding together the reactants before loading the reaction can drastically speed up this initial stage of the synthesis. Further comparison between the ground 30 and 60 min (Figure 6d) PXRD patterns shows no significant differences; this suggests that as P_2Se_5 is consumed to form a solid product, there is less liquid medium to mobilize the remaining reactants and counteract the formation of parasitic binaries and ternaries. However, increased flux amounts would alleviate this issue. Most importantly, this experiment demonstrated that given a sufficiently oxidizing P_2Se_5 flux environment, some $M_2P_2Se_6$ compounds can be synthesized in as quickly as 30 min.

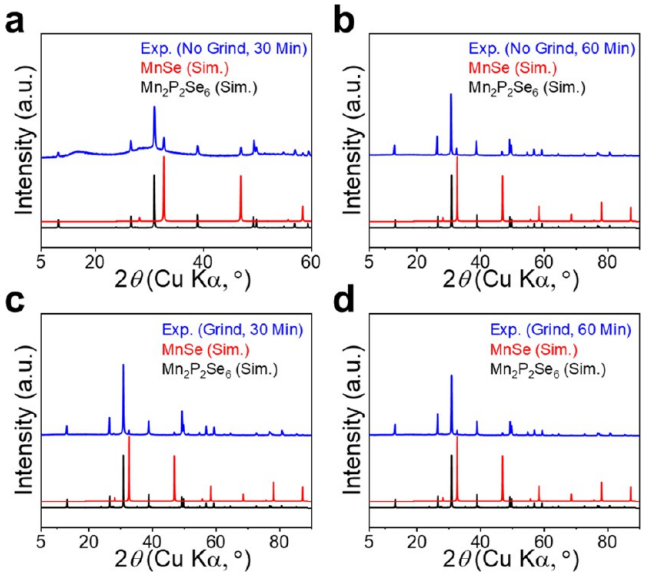

Figure 6. PXRD patterns of polycrystalline $Mn_2P_2Se_6$ ingots rapidly synthesized by loading ∼1 g reactions of Mn powder, Se powder, and P_2Se_5 pieces (25−50 mm^3) (a) not ground together and heated for 30 min, (b) not ground together and heated for 60 min, (c) ground together to a fine powder and heated for 30 min, and (d) ground together to a fine powder and heated for 60 min in a furnace pre-heated to 650 °C. P_2Se_5 and MnSe are consumed to form $Mn_2P_2Se_6$, expedited if the reactants are pre-ground before loading the reaction.

Synthesis of Layered Metal Selenophosphate Crystals. Following the successful rapid synthesis of various $M_2P_2Se_6$ powders, further exploration into the synthesis of $M_2P_2Se_6$ crystals was done. Despite a 2 M: 3 P_2S_5 ratio being sufficient to grow layered metal thiophosphate crystals, it appeared that a 2 M: 3 P_2Se_5 ratio was not sufficient to grow layered metal selenophosphate crystals. This was not wholly unexpected—in comparison to other flux-mediated syntheses in the literature, a reactant-to-flux ratio of 2:3 is comparatively low.[47,48] Thus, Mn/P_2Se_5 reactions with increased P_2Se_5 amounts were tested: metal-to-P_2Se_5 ratios of 2:3, 2:9, and 2:15 were tested using the standard heating profile shown in Figure 2a, with $Mn_2P_2Se_6$ as the target product. Visually, there were no discernible differences in crystallite size among the three reactions.

During P_2S_5 and P_2Se_5 flux removal by distillation, it was observed that at the same temperature, molten P_2Se_5 was more viscous than molten P_2S_5; it was hypothesized that conducting reactions at temperatures above 650 °C could improve the mobility of the liquid flux. This prompted an additional trial of the 2 Mn:15 P_2Se_5 ratio at an increased temperature of 800 °C (Figure 2b). This experiment produced orange $Mn_2P_2Se_6$ flakes approximately 1 mm^2 in areal dimension. It was then investigated if extending the annealing or cooling durations would improve the crystallization; annealing and cooling durations were quadrupled to 96 h instead of the initial 24 h periods (Figure 2h,i)—neither variable change visually improved $Mn_2P_2Se_6$ crystal quality or size, so it was determined that a 24 h dwell at 800 °C and 24 h cooling period would be sufficient (Figure 2b) for further exploration of other $M_2P_2Se_6$/$MM'P_2Se_6$ material syntheses.

Monometallic reactions Mg/P_2Se_5, Cr/P_2Se_5, Fe/P_2Se_5, Ni/P_2Se_5, Zn/P_2Se_5, and Cd/P_2Se_5 were also investigated, using a 2 M: 15 P_2Se_5 ratio, heated under the same conditions as those of the $Mn_2P_2Se_6$ crystal synthesis (Figure 2b). From this method, large (>1 mm^2) flakes of $Mn_2P_2Se_6$, $Fe_2P_2Se_6$, and $Cd_2P_2Se_6$ were also produced (Figure 5a−c). $Zn_2P_2Se_6$ was synthesized as a cluster of flakes (Figure S8a), molded to the shape of the reaction tube. The Cr/P_2Se_5 reaction produced small crystallites of $Cr_2P_2Se_6$. The Ni/P_2Se_5 reaction only produced $NiSe_2$.

https://doi.org/10.1021/acs.chemmater.3c00342
Chem. Mater. 2023, 35, 3671−3685

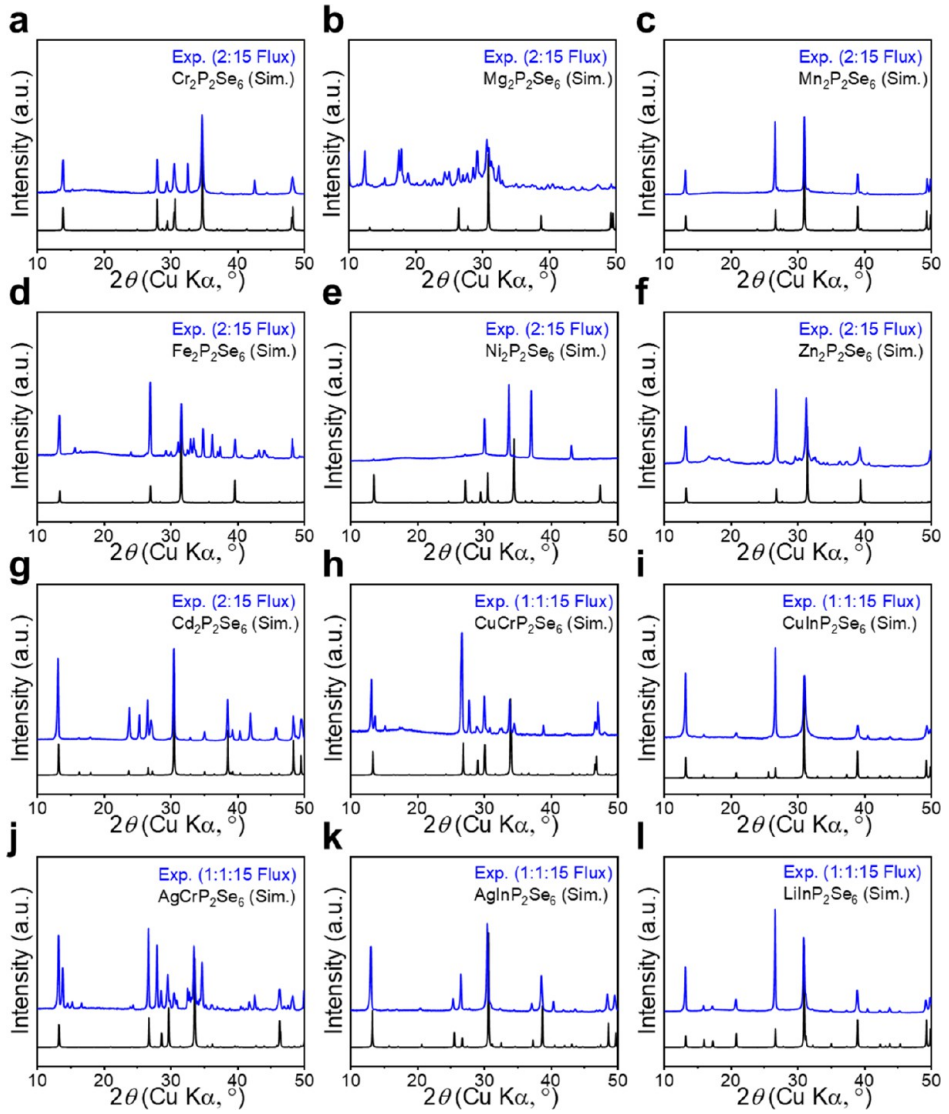

Figure 7. Monometallic and bimetallic selenophosphate PXRD comparisons between simulated patterns (in black) and experimental patterns (black) obtained from reactions using the heating profile from Figure 2b for (a) $Cr_2P_2Se_6$ (Cr_2Se_3 impurity), (b) $Mg_2P_2Se_6$ (P_4Se_3 and MgP_4 impurities), (c) $Mn_2P_2Se_6$, (d) $Fe_2P_2Se_6$ ($FeSe_2$, Fe_3Se_2, and Fe_3Se_4 impurities), (e) $Ni_2P_2Se_6$ (complete formation of $NiSe_2$), (f) $Zn_2P_2Se_6$ (P_xSe_y impurities), (g) $Cd_2P_2Se_6$ (CdSe impurity), (h) $CuCrP_2Se_6$ (Cu_3PSe_4, Cr_2Se_3, and $Cr_2P_2Se_6$ impurities), (i) $CuInP_2Se_6$, (j) $AgCrP_2Se_6$ ($Ag_4P_2Se_6$, Cr_2Se_3, and $Cr_2P_2Se_6$ impurities), (k) $AgInP_2Se_6$, and (l) $LiInP_2Se_6$.

Various bimetallic selenophosphates were also explored using $M/M'/P_2Se_5$ ratios of 1:1:15 and heating with the profile shown in Figure 2b. These reactions resulted in large (>1 mm^2) flakes of $CuCrP_2Se_6$, $CuInP_2Se_6$, $AgCrP_2Se_6$, and $AgInP_2Se_6$ (Figure 5e–h, respectively). $LiInP_2Se_6$ was also investigated by combining $Li_2Se/In/P_2Se_5$ in a 0.5:1:15 ratio, similarly growing large flakes of $LiInP_2Se_6$ (Figure 5i). Other than $Mg_2P_2Se_6$, which degraded in less than a minute of air exposure, crystal flakes of layered metal selenophosphates grown by this method showed no visible degradation after several months of storage in an ambient atmosphere. Detailed synthesis procedures are provided in the Supporting Information.

In comparison to the previous reactions that formed powder or polycrystalline products, these reactions generally produced a greater percentage of impurities. Basic PXRD pattern comparisons between observed and simulated patterns are shown in Figure 7; detailed identifications of the impurities in each reaction are provided in Figure S8. Of the 11 reactions that successfully formed their target compounds in the powder or polycrystalline form, only 3 continued to produce phase-pure products: $Mn_2P_2Se_6$, $AgInP_2Se_6$, and $CuInP_2Se_6$. However, in every reaction that produced crystalline flakes, the target $M_2P_2Se_6/MM'P_2Se_6$ phases could be mechanically separated from the rest of the reaction product. As a demonstration, pure $Fe_2P_2Se_6$ and $AgCrP_2Se_6$ flakes were removed from their highly contaminated reactions, ground into a powder, and then compositionally analyzed through PXRD and Rietveld refinement (Figures S12 and S21).

As further verification of crystal quality, PXRD was run on selected flakes of $Fe_2P_2Se_6$, $LiInP_2Se_6$, $CuInP_2Se_6$, and $AgInP_2Se_6$ in order to analyze Gauss peak fits of (00*l*) Bragg's reflections; lower fwhm values indicate less variation in the unit cells present in the sample (Figure S32).

Lattice Parameters and Unit Cell Volumes from Rietveld Refinements. Rietveld refinements of the PXRD data were conducted using GSAS II[40] in order to verify the lattice parameters of monometallic and bimetallic selenophos-

https://doi.org/10.1021/acs.chemmater.3c00342
Chem. Mater. 2023, 35, 3671−3685

Table 2. Refined Lattice Parameters from Rietveld Refinement of PXRD Patterns Taken of Monometallic and Bimetallic Selenophosphates at Room Temperature[a]

compound	a (Å)	b (Å)	c (Å)	β	cell volume (Å^3)
$Mg_2P_2Se_6$ ($R\bar{3}h$)[29]	6.3924(3)	6.3924(3)	20.1460(9)		712.93(6)
$Cr_2P_2Se_6$ ($C2/m$)[51]	6.150(2)	10.6050(7)	6.684(3)	107.742(7)	415.21(5)
$Mn_2P_2Se_6$ ($R\bar{3}h$)[51]	6.3797(2)	6.3797(2)	20.0235(4)		705.78(3)
$Fe_2P_2Se_6$ ($R\bar{3}h$, powder)[51]	6.2571(3)	6.2571(3)	19.7991(5)		671.31(5)
$Fe_2P_2Se_6$ ($R\bar{3}h$, flake)[51]	6.254(1)	6.254(1)	19.863(2)		672.8(2)
$Ni_2P_2Se_6$ ($C2/m$)[51]	6.130(2)	10.6174(8)	6.868(2)	107.423(7)	426.51(5)
$Zn_2P_2Se_6$ ($R\bar{3}h$)[29]	6.2870(4)	6.2870(4)	19.9337(8)		682.34(5)
$Cd_2P_2Se_6$ ($R\bar{3}h$)[51]	6.5076(1)	6.5076(1)	20.0564(4)		735.57(3)
$LiInP_2Se_6$ ($P\bar{3}1c$)[52]	6.4032(6)	6.4032(6)	13.3483(6)		473.97(7)
$CuCrP_2Se_6$ ($C2/m$)[37]	6.214(2)	10.7611(9)	6.935(2)	107.168(6)	443.06(4)
$AgCrP_2Se_6$ ($C2/m$, polycrystalline)[37]	6.311(2)	10.932(1)	6.999(2)	107.746(7)	459.90(5)
$AgCrP_2Se_6$ ($C2/m$, flake)[37]	6.312(2)	10.938(1)	7.004(3)	107.847(8)	460.28(7)
$AgInP_2Se_6$ ($P\bar{3}1c$)[37]	6.4734(6)	6.4734(6)	13.3216(6)		483.45(6)
$CuInP_2Se_6$ ($P\bar{3}1c$)[37]	6.386(1)	6.386(1)	13.340(1)		471.1(1)

[a]Published space groups are provided in parentheses following each compound.

phates and compare them to published literature values. Refined lattice parameters are compiled in Table 2. Rietveld refinement plots and statistics are available in the Supporting Information. Like the metal thiophosphates, the metal selenophosphates within the same space groups generally display a trend of decreased cell volume as with the increased Z value across the periodic row and down the columns, suggesting that the ionic radius of the metal is the primary determinant of the unit cell volume in all three a, b, and c directions. For example, the unit cell volumes of $Mn_2P_2Se_6$, $Fe_2P_2Se_6$, and $Zn_2P_2Se_6$ proceed in the following order: $Mn_2P_2Se_6$ > $Zn_2P_2Se_6$ > $Fe_2P_2Se_6$, in accordance with decreasing octahedral ionic radii, as reported by Shannon et al.[49]

Commenting on this in depth, Susner et al. investigated trends in P−P bond distance and layer thicknesses against effective cation radii. Specifically for $M_2P_2S_6$ compounds, they found that P−P bond lengths were highly correlated with average effective cation radii, which, in turn, were highly correlated with $M_2P_2S_6$ layer thicknesses. For $M_2P_2Se_6$ compounds, the P−P bond lengths had a V-shaped correlation with effective cation radii (smallest and largest cation radii resulted in longer P−P bond lengths) and that the correlation between P−P bond lengths and $M_2P_2Se_6$ layer thicknesses was much weaker. However, despite this, the effective cation radii actually had a stronger correlation with the layer thicknesses in $M_2P_2Se_6$ compounds than that in $M_2P_2S_6$ compounds.[22] In accordance with crystal field theory, it could be hypothesized that if the strength of the polarized Se ligands can produce a sufficiently large split in the crystal field, then the low-spin octahedral Mn^{2+} would have a smaller ionic radius than an octahedral Mg^{2+} cation.

Caution must be used when making such comparisons: in the bimetallic layered metal selenophosphates and speculatively in some monometallic layered metal selenophosphates such as $Cd_2P_2Se_6$, some metals prefer to reside off-center to the octahedral pocket.[2,22] It is also important to note that unlike the layered metal thiophosphates, which predominantly belong to the $C2/m$ space group, layered metal selenophosphates also have a multitude of members that belong to the $R\bar{3}$ space group.

SEM−EDS Analysis of Bimetallic $MM'P_2Se_6$ Flakes. Bimetallic $MM'P_2Se_6$ flakes were analyzed with SEM−EDS to verify their compositions (Figure 8). All bimetallic $MM'P_2Se_6$ flakes were confirmed to have effective M/M′/P/Se ratios of

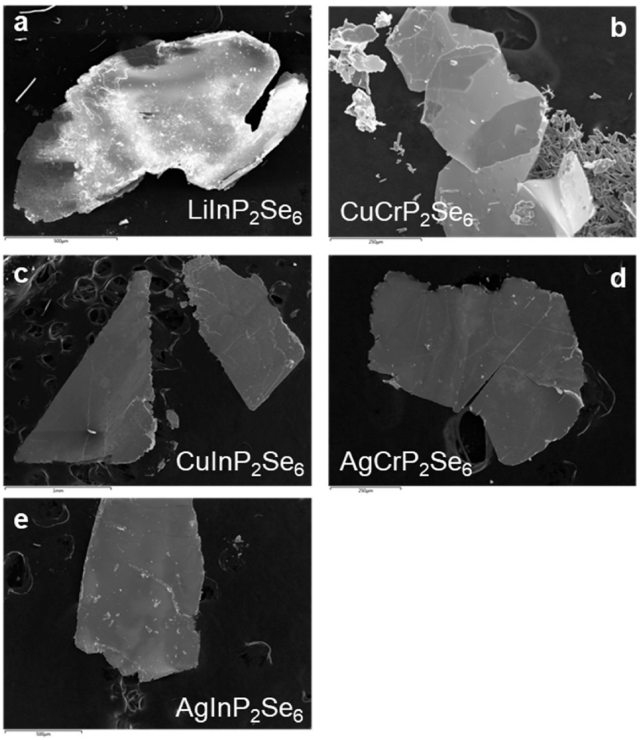

Figure 8. SEM images of bimetallic $MM'P_2Se_6$ flakes and the locations used for SEM−EDS analysis: (a) $LiInP_2Se_6$, (b) $CuCrP_2Se_6$, (c) $CuInP_2Se_6$, (d) $AgCrP_2Se_6$, and (e) $AgInP_2Se_6$. SEM−EDS was used to help confirm the compositions of synthesized crystals.

1:1:2:6 (Table 3). Samples including In demonstrated lower standard deviations in elemental compositions than samples with Cr as the secondary 3+ metal cation. This difference in variation appears to reflect real chemical variation. It was observed that the In-containing bimetallic compounds formed much more easily and with better crystal quality than the Cr-containing bimetallic compounds. This could be related to hard−soft acid−base theory; In^{3+} is much softer than Cr^{3+} and thus could react more favorably with soft $[P_2Se_6]^{4-}$ units.

https://doi.org/10.1021/acs.chemmater.3c00342
Chem. Mater. 2023, 35, 3671−3685

Table 3. Calculated Stoichiometries of Each Element Present in the $MM'P_2Se_6$ Flakes Analyzed by SEM−EDS, with Standard Deviation from the Mean in Parentheses

compound	M	M′	P	Se
$CuCrP_2Se_6$	0.987 (0.089)	0.9883 (0.058)	2.155 (0.146)	5.870 (0.124)
$AgCrP_2Se_6$	1.041 (0.025)	0.968 (0.067)	2.035 (0.080)	5.955 (0.018)
$LiInP_2Se_6$	N/A	1.002 (0.019)	2.019 (0.029)	5.979 (0.022)
$CuInP_2Se_6$	1.037 (0.043)	0.979 (0.020)	2.008 (0.043)	5.976 (0.037)
$AgInP_2Se_6$	1.005 (0.023)	1.016 (0.004)	1.984 (0.025)	5.994 (0.030)

Alternatively, it is possible that the bimetallic materials form by Cu/Ag reacting with already formed $M_xP_2Se_6$. It is possible that the formation of the structure type depends on the stability of the metals' oxidation state and a preference to fully occupy the octahedral sites, which can compete in specific cases. For example, $In_{4/3}P_2Se_6$ does exist, likely due to the preference for the In^{3+} oxidation state.[22] However, the preference for Cr^{3+} over Cr^{2+} in the reducing environment of P_2Se_5 flux may not outrank the preference for the structure to have all of the octahedral sites filled with metal cations, causing the Cr/P_2Se_5 system to preferentially form $Cr_2P_2Se_6$. If the reaction between Cu/Ag and $In_{4/3}P_2Se_6$ was more favorable than the reaction between Cu/Ag and $Cr_2P_2Se_6$, then this could account for the lower homogeneity and crystal quality of the $M^ICrP_2Se_6$ samples.

This investigation would greatly benefit from in situ PXRD measurements comparing the $Ag/Cr/P_2Se_5$ system to the $Ag/In/P_2Se_5$ system.

TEM Imaging, SAED, and STEM−EDS. TEM bright field (BF) reveals the strain contrast in each representative flake of $Mn_2P_2Se_6$, $Fe_2P_2Se_6$, and $AgInP_2Se_6$ due to the exfoliation and deposition process onto the TEM grids (Figure 9a−c). The SAED pattern taken perpendicular to the *ab*-plane/along the *c*-axis of $Mn_2P_2Se_6$, $Fe_2P_2Se_6$, and $AgInP_2Se_6$ (Figure 9d−f) shows nearly perfect sets of rotational symmetry patterns of a hexagonal crystal, indicating that the flakes were single crystals with minimal defects. All simulated SAED patterns agree with respective experimental SAED patterns (Figure S29). It is interesting to note the observation of extra diffraction spots in the $Fe_2P_2Se_6$ sample which in Figure S29b is represented by crosses. These extra spots are likely due to deviations from the expected ordering of the cation species within its octahedral site as they should be systematic (lattice) absences with no intensity. Further single crystal studies will be conducted to understand the ordering of each respective cation and anion species. The HRTEM images taken from thin regions near the edge of each representative flake shown in Figure 9a−c are shown in Figure 9g−i with $(3\bar{3}00)$ and $(03\bar{3}0)$ lattice planes indicated. The indices as described have 4 directions as $Mn_2P_2Se_6$, $Fe_2P_2Se_6$, and $AgInP_2Se_6$ are previously reported to be trigonal systems.[26,30]

High-angle annular dark-field images of each respective flake of $Mn_2P_2Se_6$, $Fe_2P_2Se_6$, and $AgInP_2Se_6$ are shown in Figure S30a−c, respectively. Local stoichiometry and chemical uniformity of the $Mn_2P_2Se_6$, $Fe_2P_2Se_6$, and $AgInP_2Se_6$ flakes

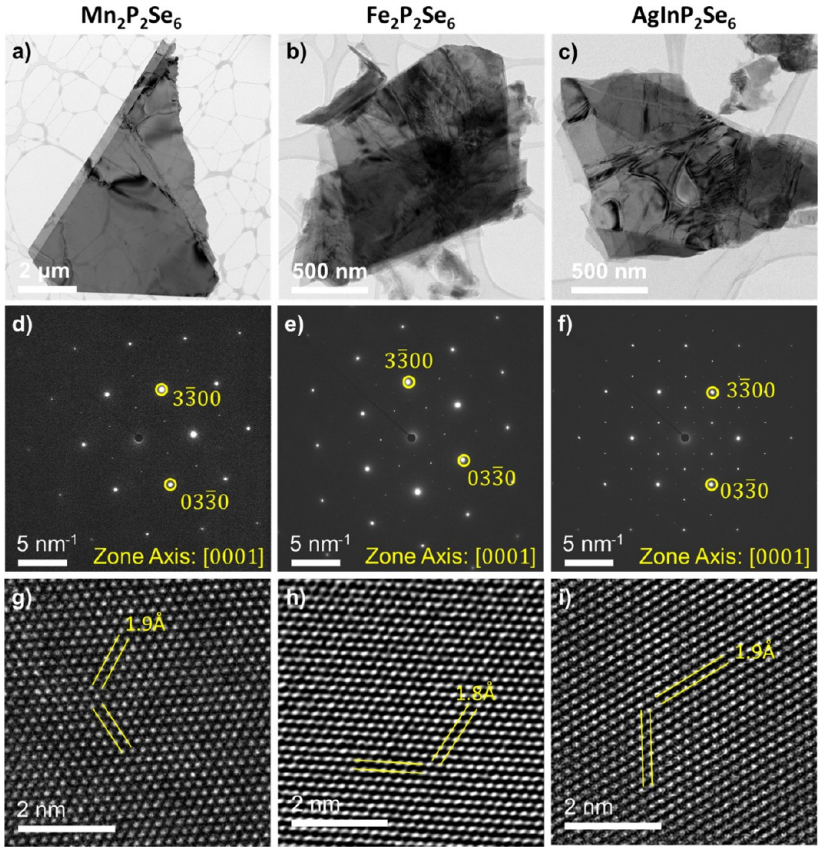

Figure 9. (a−c) BF-TEM image for $Mn_2P_2Se_6$, $Fe_2P_2Se_6$, and $AgInP_2Se_6$, respectively. (d−f) SAED for $Mn_2P_2Se_6$, $Fe_2P_2Se_6$, and $AgInP_2Se_6$, respectively. (g−i) HRTEM image for $Mn_2P_2Se_6$, $Fe_2P_2Se_6$, and $AgInP_2Se_6$, respectively.

https://doi.org/10.1021/acs.chemmater.3c00342
Chem. Mater. 2023, 35, 3671−3685

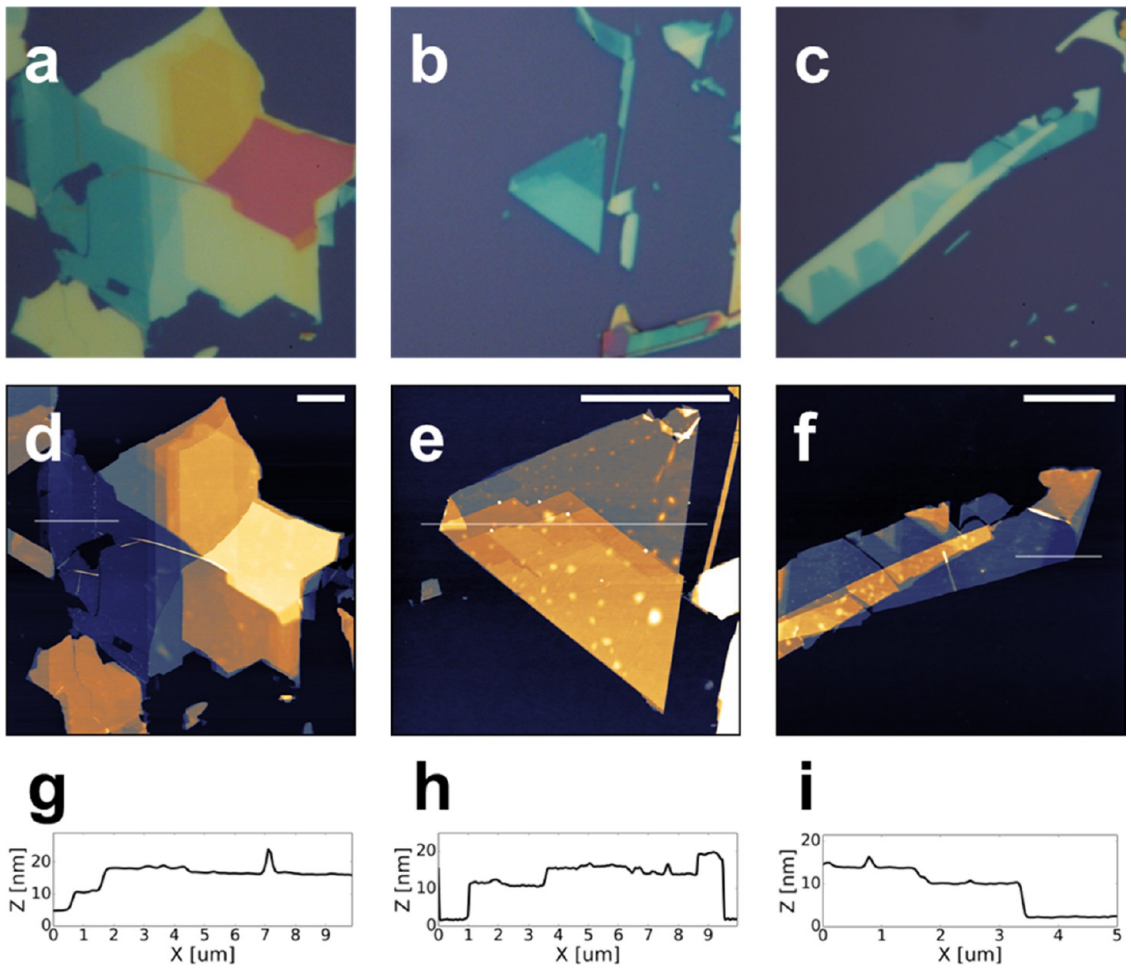

Figure 10. Mechanically exfoliated crystal flakes of (a,d) $Mn_2P_2Se_6$, (b,e) $Fe_2P_2Se_6$, and (c,f) $AgInP_2Se_6$, on 285 nm Si oxide-capped Si wafers. AFM maps of the (g) $Mn_2P_2Se_6$, (h) $Fe_2P_2Se_6$, and (i) $AgInP_2Se_6$ flakes, showing thicknesses of the exfoliated films.

are evaluated using STEM−EDS mapping, where the colored maps denoting P in red, Se in yellow, Mn in magenta, Fe in orange, Ag in blue, and In in green show a homogeneous EDS signal throughout each respective system. The measured nominally proportional stoichiometry of $Mn_2P_2Se_6$, $Fe_2P_2Se_6$, and $AgInP_2Se_6$ is shown in Table S7, match is very close to the expected values. Together with the SAED pattern confirms the formation of single crystals of $Mn_2P_2Se_6$, $Fe_2P_2Se_6$, and $AgInP_2Se_6$.

Exfoliation of Bimetallic Selenophosphates. Similar to the thiophosphate analogues, metallic selenophosphates exfoliate readily into thin films via mechanical exfoliation. Large single crystals can be exfoliated with ease into ∼10−100 nm thick flakes using conventional "scotch tape" methods and show a strong optical contrast on 285 and 90 nm Si oxide substrates (Figure 10a−c) which is required for optical identification of thin vdW films for characterization and use in vdW heterostructure assembly. To demonstrate the viability of the bulk crystals grown by this method for exfoliation studies, crystals were mechanically exfoliated using PVC tape (Nitto Denko brand) onto 285 nm Si oxide-capped Si wafers, shown in Figure 10d−f. Optically, the flakes show strong layer contrast and form large flakes which do not break up significantly, indicating relatively high stability under ambient conditions. Atomic force microscopy (AFM) maps of the flakes (Figure 10g−i), measured on a Park XE-150 AFM in the contact mode immediately after exfoliation indicate that sharply layered continuous films <20 nm thick are obtained, with micron-sized regions as thin as 5 nm thick being present. We note that the amorphous surface texture on the $Fe_2P_2Se_6$ and $AgInP_2Se_6$ films is consistent with adhesive residue commonly seen in mechanically exfoliated films. Charge transport investigation was attempted on compounds including $Mn_2P_2Se_6$, which showed an expected Mott insulator behavior at room temperature with micron-size exfoliated film devices showing resistance in excess of 100 GΩ. Such high resistance may be desirable in certain electronic applications or by use as an encapsulant in vdW heterostructure devices. For all films, we observe no visible degradation in air over time.

Photoemission Yield Spectroscopy in Air (PYSA). The work functions of the layered metal selenophosphate crystalline flakes were determined using PYSA, as shown in Figure 11. The work function values represent the energy levels of the top of the valence bands, given the wide-gap semiconducting character of these materials. They range from 5.25 to 5.72 eV, similar to the work functions observed for the layered metal thiophosphates.[35] Knowledge of the work functions of these materials is essential for selecting metal contacts in device fabrication.[50]

https://doi.org/10.1021/acs.chemmater.3c00342
Chem. Mater. 2023, 35, 3671−3685

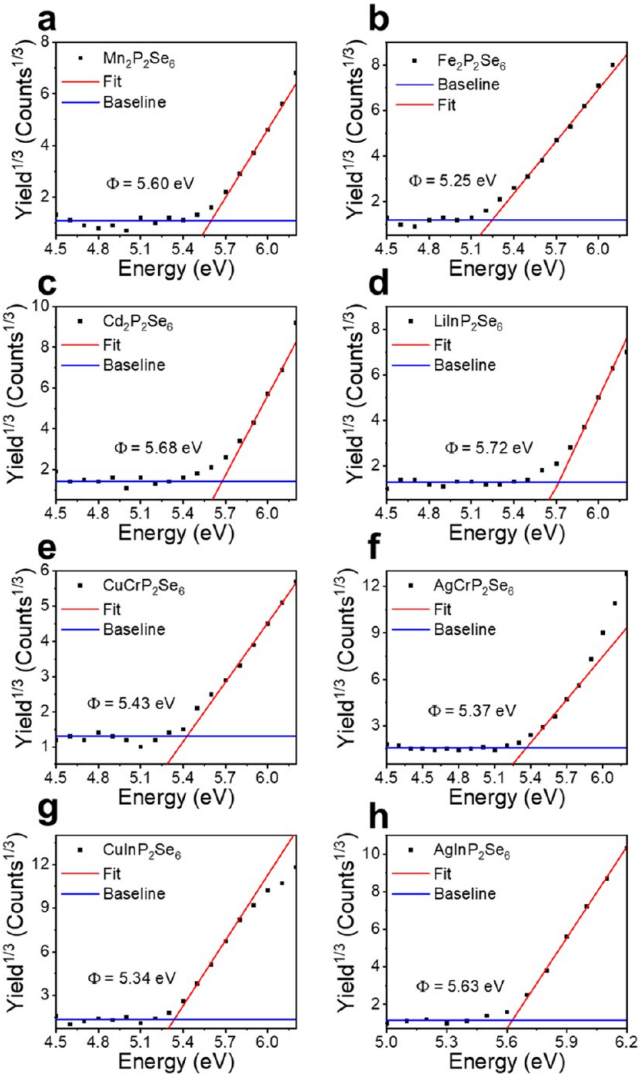

Figure 11. PYSA spectra of layered metal selenophosphate crystalline flakes. (a) $Mn_2P_2Se_6$, (b) $Fe_2P_2Se_6$, (c) $Cd_2P_2Se_6$, (d) $LiInP_2Se_6$, (e) $CuCrP_2Se_6$, (f) $AgCrP_2Se_6$, (g) $CuInP_2Se_6$, and (h) $AgInP_2Se_6$.

CONCLUSIONS

We have demonstrated that the P_2Se_5 flux as a reactive medium oxidizes metals and leads to the rapid formation of layered metal selenophosphate phases, enabling significantly shorter reaction times compared to current literature methods. We developed 60 h syntheses for a myriad of $M_2P_2Se_6$/$MM'P_2Se_6$ powders, with general guidelines for exploring rapid syntheses of other members in the family. We also developed a generalizable 60 h synthesis for $M_2P_2Se_6$/$MM'P_2Se_6$ crystalline flakes, accompanied by a P_2Se_5 flux removal method accessible to anyone with a furnace. We then verified the quality of the P_2Se_5 flux-grown crystals using a wide variety of characterization techniques, including Rietveld refinement, SEM−EDS, TEM, SAED, STEM−EDS mapping, and AFM.

It is important to note that the listed synthetic conditions are not necessarily fixed and can be modified to synthesize these compounds. Some of these compounds have been synthesized using shorter temperature profiles and pure phases, but the specific heating profile parameters such as dwelling temperatures, ramp rates, and others have not been optimized for each individual compound. Additionally, despite enhanced crystal growth at elevated temperatures, some layered metal selenophosphates also decompose at these temperatures, requiring further optimization of the dwell temperatures. Thus, we present this study as a starting point for the reader to further explore these reaction spaces or synthesize reported materials for single crystal studies.

Given the conclusion that P_2Se_5 flux helps the oxidization of metal reagents in a liquid reaction medium, it should be noted that this effect is not limited to a single metal at a time. The use of P_2Se_5 flux facilitates the dissolution and crystallization of multiple metals concurrently, as evidenced by the improved crystal growth of various bimetallic selenophosphates. The implications of this are extraordinary—not only could new combinations of $M^IM^{III}P_2Se_6$ be devised for further discovery of new ferro/ferri/antiferro/antiferrielectric systems but use of P_2Se_5 flux could be the gateway to exploring crystals of $M^{II}M'^{II}P_2Se_6$ systems. Magnetic exploration of divalent bimetallic selenophosphate systems would be quintessential for manipulating the magnetic properties of these materials. Synthesizing crystals under these conditions could allow for further single-crystal studies of divalent bimetallic selenophosphate systems, such as $CrMnP_2Se_6$, $CrFeP_2Se_6$, and $NiZnP_2Se_6$, among many other potential combinations.

ASSOCIATED CONTENT

Supporting Information

The Supporting Information is available free of charge at https://pubs.acs.org/doi/10.1021/acs.chemmater.3c00342.

Additional experimental synthesis details, SEM−EDS, P_2Se_5 distillation setup, heating profiles used for VT PXRD, additional PXRD analyses, Rietveld refinement plots and statistics, SEM images and representative spectra for bimetallic crystals, additional VT PXRD of the Co/P_2Se_5 system, simulated SAED patterns, STEM−EDS maps, and fwhm peak values of (00*l*) Bragg's reflections (PDF)

AUTHOR INFORMATION

Corresponding Author

Mercouri G. Kanatzidis − *Department of Chemistry, Northwestern University, Evanston, Illinois 60208, United States;* orcid.org/0000-0003-2037-4168; Email: m-kanatzidis@northwestern.edu

Authors

Eric K. Qian − *Department of Chemistry, Northwestern University, Evanston, Illinois 60208, United States;* orcid.org/0000-0003-2314-7569

Abishek K. Iyer − *Department of Chemistry, Northwestern University, Evanston, Illinois 60208, United States;* orcid.org/0000-0002-8582-3895

Matthew Cheng − *Department of Material Science and Engineering, Northwestern University, Evanston, Illinois 60208, United States;* orcid.org/0000-0002-1062-5974

Kevin M. Ryan − *Northwestern University Atomic and Nanoscale Characterization Experimental (NUANCE) Center, Northwestern University, Evanston, Illinois 60208, United States*

Lillian Jirousek − *Northwestern University Atomic and Nanoscale Characterization Experimental (NUANCE) Center, Northwestern University, Evanston, Illinois 60208, United States*

https://doi.org/10.1021/acs.chemmater.3c00342
Chem. Mater. 2023, 35, 3671−3685

Daniel G. Chica − *Department of Chemistry, Northwestern University, Evanston, Illinois 60208, United States;* orcid.org/0000-0001-8616-9365
Patrick Krantz − *Northwestern University Atomic and Nanoscale Characterization Experimental (NUANCE) Center, Northwestern University, Evanston, Illinois 60208, United States*
Yea-Shine Lee − *Department of Material Science and Engineering, Northwestern University, Evanston, Illinois 60208, United States;* orcid.org/0000-0002-2087-4886
Venkat Chandrasekhar − *Department of Physics and Astronomy, Northwestern University, Evanston, Illinois 60208, United States*
Vinayak P. Dravid − *Department of Material Science and Engineering, International Institute for Nanotechnology (IIN), and Northwestern University Atomic and Nanoscale Characterization Experimental (NUANCE) Center, Northwestern University, Evanston, Illinois 60208, United States;* orcid.org/0000-0002-6007-3063

Complete contact information is available at: https://pubs.acs.org/10.1021/acs.chemmater.3c00342

Notes

The authors declare no competing financial interest.

■ ACKNOWLEDGMENTS

This work was supported by the Army Research Office (grant W911NF1910335), the NSF Graduate Research Fellowship under Grant DGE-1842165, and the NSF Division of Material Research (DMR-2003476). This work made use of the EPIC facility of Northwestern University's NUANCE Center, which has received support from the Soft and Hybrid Nanotechnology Experimental (SHyNE) Resource (NSF ECCS1542205), the MRSEC program (NSF DMR-1720139) at the Materials Research Center, the International Institute for Nanotechnology (IIN), the Keck Foundation, and the State of Illinois, through the IIN. This work also made use of the IMSERC Crystallography facility at Northwestern University, which has received support from the Soft and Hybrid Nanotechnology Experimental (SHyNE) Resource (NSF ECCS-2025633) and Northwestern University. We would also like to thank C.C.L., M.A.Q., and B.M.O. for their discussions and advice.

■ REFERENCES

(1) Friedel, C. M. Soufre et ses composés—sur une nouvelle série de sulfophosphures, les thiohypophosphates. *C. r. hebdo. séances Acad. sci.* **1894**, *119*, 260−264.
(2) Gave, M. A.; Bilc, D.; Mahanti, S. D.; Breshears, J. D.; Kanatzidis, M. G. On the Lamellar Compounds $CuBiP_2Se_6$, $AgBiP_2Se_6$ and $AgBiP_2S_6$. Antiferroelectric Phase Transitions Due to Cooperative Cu^+ and Bi^{3+} Ion Motion. *Inorg. Chem.* **2005**, *44*, 5293−5303.
(3) Simon, A.; Ravez, J.; Maisonneuve, V.; Payen, C.; Cajipe, V. B. Paraelectric-Ferroelectric Transition in the Lamellar Thiophosphate $CuInP_2S_6$. *Chem. Mater.* **1994**, *6*, 1575−1580.
(4) Sun, Y.-J.; Pang, S.-M.; Zhang, J. Review of Raman spectroscopy of two-dimensional magnetic van der Waals materials. *Chinese Physics B* **2021**, *30*, 117104.
(5) Lai, Y.; Song, Z.; Wan, Y.; Xue, M.; Wang, C.; Ye, Y.; Dai, L.; Zhang, Z.; Yang, W.; Du, H.; et al. Two-dimensional ferromagnetism and driven ferroelectricity in van der Waals $CuCrP_2S_6$. *Nanoscale* **2019**, *11*, 5163−5170.
(6) Banys, J.; Macutkevic, J.; Grigalaitis, R.; Vysochanskii, J. Influence of small amount of $CuInP_2Se_6$ to conductivity of $CuInP_2S_6$ crystals. *Solid State Ionics* **2008**, *179*, 79−81.
(7) Huang, S.; Shuai, Z.; Wang, D. Ferroelectricity in 2D metal phosphorus trichalcogenides and van der Waals heterostructures for photocatalytic water splitting. *J. Mater. Chem. A* **2021**, *9*, 2734−2741.
(8) Hua, C.; Bai, H.; Zheng, Y.; Xu, Z.-A.; Yang, S. A.; Lu, Y.; Wei, S.-H. Strong Coupled Magnetic and Electric Ordering in Monolayer of Metal Thio(seleno)phosphates. *Chin. Phys. Lett.* **2021**, *38*, 077501.
(9) Ho, C.-H.; Hu, S.-F.; Chang, H.-W. Thermoreflectance characterization of the band-edge excitons observed in multilayered $CuInP_2S_6$. *FlatChem* **2021**, *29*, 100290.
(10) Liaqat, A.; Yin, Y. H.; Hussain, S.; Wen, W.; Wu, J. X.; Guo, Y. Z.; Dang, C. H.; Ho, C. H.; Liu, Z.; Yu, P.; et al. An all two-dimensional vertical heterostructure graphene/$CuInP_2S_6$/MoS_2 for negative capacitance field effect transistor. *Nanotechnology* **2022**, *33*, 125703.
(11) Kou, Z.; Wang, K.; Liu, Z.; Zeng, L.; Li, Z.; Yang, B.; Lei, L.; Yuan, C.; Hou, Y. Recent Advances in Manifold Exfoliated Synthesis of Two-Dimensional Non-precious Metal-Based Nanosheet Electrocatalysts for Water Splitting. *Small Struct.* **2021**, *3*, 2100153.
(12) Chen, K.; Liu, J.; Huang, Z.; Zong, S.; Liu, L.; Tan, W. Construction of novel 2D-0D $MnPS_3$−$Cs_4W_{11}O_{35}$ composite for the improved photocatalytic hydrogen evolution activity. *Int. J. Hydrogen Energy* **2021**, *46*, 33823−33834.
(13) Sanna, M.; Ng, S.; Pumera, M. Layered transition metal selenophosphites for visible light photoelectrochemical production of hydrogen. *Electrochem. Commun.* **2021**, *129*, 107077.
(14) Oliveira, F. M.; Paštika, J.; Pires, L. S.; Sofer, Z.; Gusmão, R. Photoelectrochemical Activity of Layered Metal Phosphorous Trichalcogenides for Water Oxidation. *Adv. Mater. Interfaces* **2021**, *8*, 2100294.
(15) Oliveira, F. M.; Paštika, J.; Mazánek, V.; Melle-Franco, M.; Sofer, Z.; Gusmão, R. Cobalt Phosphorous Trisulfide as a High-Performance Electrocatalyst for the Oxygen Evolution Reaction. *ACS Appl. Mater. Interfaces* **2021**, *13*, 23638−23646.
(16) Yu, P.; Wang, F.; Meng, J.; Shifa, T. A.; Sendeku, M. G.; Fang, J.; Li, S.; Cheng, Z.; Lou, X.; He, J. Few-layered $CuInP_2S_6$ nanosheet with sulfur vacancy boosting photocatalytic hydrogen evolution. *CrystEngComm* **2021**, *23*, 591−598.
(17) Barua, M.; Ayyub, M. M.; Vishnoi, P.; Pramoda, K.; Rao, C. N. R. Photochemical HER activity of layered metal phospho-sulfides and -selenides. *J. Mater. Chem. A* **2019**, *7*, 22500−22506.
(18) Kumar, R.; Jenjeti, R. N.; Choutipalli, V. S. K.; Subramanian, V.; Sampath, S. Conductometric NO_x sensor based on exfoliated two-dimensional layered $MnPSe_3$. *Sens. Actuators, B* **2021**, *347*, 130633.
(19) Zhao, G.; Wang, L.; Ke, X.; Yu, Z. Digital and analog memory devices based on 2D layered MPS_3 (M = Mn, Co, Ni) materials. *Chinese Physics B* **2021**, *30*, 047303.
(20) Li, Y.; Fu, J.; Mao, X.; Chen, C.; Liu, H.; Gong, M.; Zeng, H. Enhanced bulk photovoltaic effect in two-dimensional ferroelectric $CuInP_2S_6$. *Nat. Commun.* **2021**, *12*, 5896.
(21) Du, K.-z.; Wang, X.-z.; Liu, Y.; Hu, P.; Utama, M. I. B.; Gan, C. K.; Xiong, Q.; Kloc, C. Weak Van der Waals Stacking, Wide-Range Band Gap, and Raman Study on Ultrathin Layers of Metal Phosphorus Trichalcogenides. *ACS Nano* **2016**, *10*, 1738−1743.
(22) Susner, M. A.; Chyasnavichyus, M.; McGuire, M. A.; Ganesh, P.; Maksymovych, P. Metal Thio- and Selenophosphates as Multifunctional van der Waals Layered Materials. *Adv. Mater.* **2017**, *29*, 1602852.
(23) Wang, F.; Shifa, T. A.; Yu, P.; He, P.; Liu, Y.; Wang, F.; Wang, Z.; Zhan, X.; Lou, X.; Xia, F.; et al. New Frontiers on van der Waals Layered Metal Phosphorous Trichalcogenides. *Adv. Funct. Mater.* **2018**, *28*, 1802151.
(24) Bourdon, X.; Maisonneuve, V.; Cajipe, V. B.; Payen, C.; Fischer, J. E. Copper sublattice ordering in layered $CuMP_2Se_6$ (M=In, Cr). *J. Alloys Compd.* **1999**, *283*, 122−127.

(25) Le Flem, G.; Brec, R.; Ouvard, G.; Louisy, A.; Ségransan, P. J. Magnetic Interactions in the Layer Compounds MPX_3 (M = Mn, Fe, Ni; X = S, Se). *J. Phys. Chem. Solids* **1982**, *43*, 455−461.
(26) Wiedenmann, A.; Rossat-Mignod, J.; Louisy, A.; Brec, R.; Rouxel, J. Neutron diffraction study of the layered compounds $MnPSe_3$ and $FePSe_3$. *Solid State Commun.* **1981**, *40*, 1067−1072.
(27) Dedkov, Y.; Yan, M.; Voloshina, E. To the synthesis and characterization of layered metal phosphorus triselenides proposed for electrochemical sensing and energy applications. *Chem. Phys. Lett.* **2020**, *754*, 137627.
(28) Gusmão, R.; Sofer, Z.; Sedmidubský, D.; Huber, Š.; Pumera, M. The Role of the Metal Element in Layered Metal Phosphorus Triselenides upon Their Electrochemical Sensing and Energy Applications. *ACS Catal.* **2017**, *7*, 8159−8170.
(29) Jörgens, S.; Mewis, A. Die Kristallstrukturen von Hexachalcogeno-Hypodiphosphaten des Magnesiums und Zinks. *Z. fur Anorg. Allg. Chem.* **2004**, *630*, 51−57.
(30) Pfeiff, R.; Kniep, R. Quaternary selenodiphosphates(IV): $M^{I}M^{III}[P_2Se_6]$, (M^{I} =Cu, Ag; M^{III} = Cr, Al, Ga, In). *J. Alloys Compd.* **1992**, *186*, 111−133.
(31) Klingen, W.; Ott, R.; Hahn, H. Uber die Darstellung und Eigenschaften von Hexathio- und Hexaselenohypodiphosphaten. *Z. fur Anorg. Allg. Chem.* **1973**, *396*, 271−278.
(32) Momma, K.; Izumi, F. VESTA 3 for three-dimensional visualization of crystal, volumetric and morphology data. *J. Appl. Crystallogr.* **2011**, *44*, 1272−1276.
(33) Taylor, B.; Steger, J.; Wold, A.; Kostiner, E. Preparation and properties of iron phosphorus triselenide, $FePSe_3$. *Inorg. Chem.* **2002**, *13*, 2719−2721.
(34) Binnewies, M.; Glaum, R.; Schmidt, M.; Schmidt, P. *Chemical Vapor Transport Reactions*; De Gruyter, 2012.
(35) Chica, D. G.; Iyer, A. K.; Cheng, M.; Ryan, K. M.; Krantz, P.; Laing, C.; dos Reis, R.; Chandrasekhar, V.; Dravid, V. P.; Kanatzidis, M. G. P_2S_5 Reactive Flux Method for the Rapid Synthesis of Mono- and Bimetallic 2D Thiophosphates $M_{2-x}M'_xP_2S_6$. *Inorg. Chem.* **2021**, *60*, 3502−3513.
(36) Kanatzidis, M. G. Discovery-Synthesis, Design, and Prediction of Chalcogenide Phases. *Inorg. Chem.* **2017**, *56*, 3158−3173.
(37) Galdámez, A.; Manríquez, V.; Kasaneva, J.; Avila, R. E. Synthesis, characterization and electrical properties of quaternary selenodiphosphates: AMP_2Se_6 with A = Cu, Ag and M = Bi, Sb. *Mater. Res. Bull.* **2003**, *38*, 1063−1072.
(38) McCarthy, T. J.; Kanatzidis, M. G. Synthesis in Molten Alkali Metal Polyselenophosphate Fluxes: A New Family of Transition Metal Selenophosphate Compounds, $A_2MP_2Se_6$ (A = K, Rb, Cs; M = Mn, Fe) and $A_2M'_2P_2Se_6$ (A = K, Cs; M' = Cu, Ag). *Inorg. Chem.* **2002**, *34*, 1257−1267.
(39) Macrae, C. F.; Sovago, I.; Cottrell, S. J.; Galek, P. T. A.; McCabe, P.; Pidcock, E.; Platings, M.; Shields, G. P.; Stevens, J. S.; Towler, M.; et al. Mercury 4.0: from visualization to analysis, design and prediction. *J. Appl. Crystallogr.* **2020**, *53*, 226−235.
(40) Toby, B. H.; Von Dreele, R. B. GSAS-II: the genesis of a modern open-source all purpose crystallography software package. *J. Appl. Crystallogr.* **2013**, *46*, 544−549.
(41) Palmer, D. C. SingleCrystal 4: real-time multi-phase diffraction simulation. *J. Appl. Crystallogr.* **2020**, *53*, 860.
(42) Jörgens, S. *Untersuchungen von Chalcogenophosphaten und Chalcogenophosphathalogeniden*; Heinrich-Heine-Universität Düsseldorf: Düsseldorf, 2004.
(43) Aitken, J. A.; Brown, S.; Chondroudis, K.; Jobic, S.; Brec, R.; Kanatzidis, M. G. β-$Bi_4(P_2Se_6)_3$: A New Ternary Selenophosphate Obtained in a P2Se5 Flux. *Inorg. Chem.* **1999**, *38*, 4795−4800.
(44) Clément, R.; Lagadic, I.; Léaustic, A.; Audière, J. P.; Lomas, L. Non-Redox Intercalation into the MPS_3 Lamellar Materials: Chemistry and Physical Properties. *Chemical Physics of Intercalation II*; NATO ASI Series, 1993; pp 315−324.
(45) Clement, R.; Lomas, L.; Audiere, J. P. Intercalation chemistry of layered iron trithiohypophosphate ($FePS_3$). An approach toward insulating magnets below 90 K. *Chem. Mater.* **1990**, *2*, 641−643.
(46) Monteil, Y.; Vincent, H. Ternary Red-Phosphorus-Sulphur-Selenium System. 2. Polythermal Diagram. *Bull. Soc. Chim. Fr.* **1975**, 1029−1033.
(47) Khoury, J. F.; Rettie, A. J. E.; Robredo, I.; Krogstad, M. J.; Malliakas, C. D.; Bergara, A.; Vergniory, M. G.; Osborn, R.; Rosenkranz, S.; Chung, D. Y.; et al. The Subchalcogenides Ir_2In_8Q (Q = S, Se, Te): Dirac Semimetal Candidates with Re-entrant Structural Modulation. *J. Am. Chem. Soc.* **2020**, *142*, 6312−6323.
(48) Zaikina, J. V.; Griffin, V. S.; Latturner, S. E. Switching on a Spin Glass: Flux Growth, Structure, and Magnetism of $La_{11}Mn_{13-x-y}Ni_xAl_ySn_{4-\delta}$ Intermetallics. *Inorg. Chem.* **2017**, *56*, 15194−15202.
(49) Shannon, R. D. Revised effective ionic radii and systematic studies of interatomic distances in halides and chalcogenides. *Acta Crystallogr., Sect. A* **1976**, *32*, 751−767.
(50) Moun, M.; Singh, R. Metal−semiconductor interface engineering in layered 2D materials for device applications. *Bull. Mater. Sci.* **2021**, *44*, 223.
(51) Brec, R.; Ouvrard, G.; Louisy, A.; Rouxel, J. Structural-Properties of the $M^{II}PS_3$, $M^{II}PSe_3$ Phases. *Ann. Chim.—Sci. Mat.* **1980**, *5*, 499−512.
(52) Chica, D. G.; He, Y.; McCall, K. M.; Chung, D. Y.; Pak, R. O.; Trimarchi, G.; Liu, Z.; De Lurgio, P. M.; Wessels, B. W.; Kanatzidis, M. G. Direct thermal neutron detection by the 2D semiconductor $^6LiInP_2Se_6$. *Nature* **2020**, *577*, 346−349.

https://doi.org/10.1021/acs.chemmater.3c00342
Chem. Mater. 2023, 35, 3671−3685